J. metamorphic Geol., 2006, **24,** 477–496 doi:10.1111/j.1525-1314.2006.00649.x

Reconstructing *P–T* paths during continental collision using multi-stage garnet (Gran Paradiso nappe, Western Alps)

B. LE BAYON,[1] P. PITRA,[1] M. BALLEVRE[1] AND M. BOHN[2]
[1]*Equipe Lithosphère, Géosciences Rennes (UMR-CNRS 6118), Université de Rennes 1, F-35042 Rennes Cedex, France (benjamin.lebayon@univ-rennes1.fr)*
[2]*Microsonde Ouest, IFREMER and CNRS, Centre de Brest, BP70, F-29280, Plouzané, France*

ABSTRACT Garnet–chloritoid-bearing micaschists from the Gran Paradiso massif (Western Alps) contain evidence of a polymetamorphic evolution. Detailed textural observations reveal that two stages of garnet growth are present in the micaschists, interpreted as: (i) relics of an early metamorphism of pre-Alpine age and (ii) newly grown Alpine garnet, respectively. Both generations of garnet preserve growth zoning. From THERMOCALC-based numerical modelling of mineral assemblages in pressure–temperature (*P–T*) pseudosections, we infer that garnet 1 grew at increasing temperature and slightly increasing pressure, whereas garnet 2 grew at decreasing pressure and slightly increasing temperature. Estimated *P–T* conditions are ~620 °C, 6 kbar for the peak of the pre-Alpine event, and of 490 °C, 18–20 kbar for the pressure peak of the Alpine event. Modelling of the modal proportion and chemical composition of garnet (i) shows that the subsequent decompression (to 14–15 kbar at 550 °C) must have been accompanied by moderate heating and (ii) does not support a stage of final temperature increase following decompressional cooling. This argues against a late thermal pulse associated with mantle delamination. Preservation of growth zoning in both generations of garnet and the limited amount of diffusive re-equilibration at the boundary between the two garnets suggests that the rocks were subjected to fast burial and exhumation rates, consistent with data obtained from other internal Alpine units.

Key words: Gran Paradiso; multi-stage garnet; *P–T* history; pseudosections; Western Alps.

INTRODUCTION

Most collision zones involve slices of continental crust that have been reworked during several, possibly unrelated, episodes. During the later metamorphic episodes, relics of the early history are progressively erased. However, traces of earlier metamorphic stages can be preserved either in low-strain domains, or within relic prekinematic phases in high-strain domains (e.g. garnet). Therefore, identification of several growth stages of garnet porphyroblasts is a potential tool for deciphering such complex histories.

Criteria for recognizing multi-stage garnet include: (i) overgrowths on preexisting grains; (ii) a bimodal grain-size distribution; (iii) differences in the geometry and/or nature of phases included in the two types of garnet; and (iv) chemical discontinuities at the boundary between garnet cores and their overgrowths, or systematic chemical differences between the two size classes of garnet crystals within a single rock (Rumble & Finnerty, 1974; Karabinos, 1984; von Raumer & Schwander, 1985; Madhjoub *et al.*, 1997; Dachs & Proyer, 2001; Faryad & Hoinkes, 2003; Vry *et al.*, 2004; Faryad & Chakraborty, 2005). However, with increasing temperature, intracrystalline diffusion within garnet (Tracy, 1982; Loomis, 1983; Robinson, 1991) tends to erase both the chemical difference between garnet grains and the chemical discontinuity between garnet cores and rims. Moreover, inclusions in the garnet may also be chemically re-equilibrated or may react with their host (Whitney, 1991; Perchuk *et al.*, 2005).

In this study, we describe metapelite samples from Gran Paradiso, in the internal zones of the Western Alps. The samples contain multi-stage garnet that has been previously used to infer: (i) a polycyclic history of the Pennine basement, i.e. eclogite facies parageneses of Alpine age overprinting the earlier, pre-Alpine (Variscan) assemblages and (ii) a late temperature increase during decompression (Borghi *et al.*, 1985; Sandrone & Borghi, 1992; Borghi & Sandrone, 1995; Borghi *et al.*, 1996), potentially caused by mantle delamination (Brouwer *et al.*, 2004). Our aim is (i) to assess how suitable multi-stage garnet is to yield information about the *P–T* evolution of polymetamorphic rocks, and (ii) to better constrain the shape of the pressure–temperature (*P–T*) path followed by the Gran Paradiso rocks and the *P–T* conditions of both metamorphic events using calculated phase diagrams.

GEOLOGICAL SETTING

The Western Alps

The Western Alps result from the collision of a southern (Adriatic) plate with a northern (European) plate, initially separated by the Piemont-Ligurian Ocean. After subduction of the oceanic crust, the distal part of the European palaeomargin (the Penninic units), as well as slices of the Adriatic margin (the Austroalpine units), were buried at moderate to great depths. Consequently, eclogite facies metamorphism took place in portions of both the Penninic and the Austroalpine units, reworking the former pre-Alpine basement. The overall pattern of the Alpine metamorphism is characterized by an eastward increase of metamorphic grade (Bertrand, 1894; Ernst, 1973; Frey *et al.*, 1974; Desmons *et al.*, 1999a).

Evidence for the polymetamorphic history of the continental crust (Fig. 1) has been reported in several units from the Western Alps. In the external zone, most of the pre-Alpine basement is left undeformed or was reworked along narrow shear zones taking place at sub-greenschist to greenschist facies conditions (Choukroune & Gapais, 1983; Leloup *et al.*, 2005). Consequently, the *P–T* history of the pre-Alpine basement in the external zone is well understood, e.g. in the Aiguilles Rouges massif (von Raumer & Bussy, 2004), the Belledonne massif, or the Argentera massif (Rubatto *et al.*, 2001).

Overprinting of the pre-Alpine metamorphism becomes more intense towards the East, in the internal (Penninic and Austroalpine) Alpine zones. In the external Penninic units (i.e. the Briançonnais–Grand Saint Bernard), greenschist facies to blueschist facies parageneses overprint the pre-Alpine basement. In some cases, the pre-Alpine mineral assemblages are well preserved (Desmons & Ghent, 1977; Desmons, 1992; Desmons *et al.*, 1999b), like in the garnet–staurolite–biotite-bearing metapelites from the Sapey (Detraz & Loubat, 1984) and Mont Mort (Burri, 1983; Thélin, 1992; Giorgis *et al.*, 1999) areas. In some cases, the Alpine metamorphic overprint is recorded by a new stage of garnet growth, like in the Ruitor massif (Desmons *et al.*, 1977; Laduron & Desmons, 1981), the Valsavarenche area (Malusà, 2005) and the Ambin massif (Ganne *et al.*, 2003).

In more internal Penninic units (Monte Rosa, Gran Paradiso, Dora-Maira), eclogite facies parageneses developed during the Alpine history (Dal Piaz & Lombardo, 1986). Pre-Alpine relics are preserved either in low-strain domains (Bearth, 1952; Dal Piaz, 1966; Compagnoni & Lombardo, 1974; Le Bayon & Ballèvre, 2006) or as prekinematic porphyroclasts in high-strain domains. Multi-stage garnet has been reported in some micaschists (Dal Piaz, 1963; Borghi *et al.*, 1985; Sandrone & Borghi, 1992; Bouffette *et al.*, 1993; Borghi *et al.*, 1996; Matsumoto & Hirajima, 2000; Le Bayon, 2003).

Finally, in the Austroalpine basement, rare relics of high-grade pre-Alpine rocks survived the Alpine eclogite facies event (Compagnoni, 1977; Lardeaux *et al.*, 1982; Hy, 1984; Vuichard & Ballèvre, 1988; Lardeaux & Spalla, 1991; Rebay & Spalla, 2001) and some micaschists display multi-stage garnet (Compagnoni, 1977; Dal Piaz *et al.*, 1983; Hy, 1984; Faryad & Chakraborty, 2005).

The Gran Paradiso Massif

The Gran Paradiso massif (like the Dora-Maira and Monte Rosa massifs) is a large tectonic window, which consists of a subducted continental crust underlying eclogite facies oceanic units. The northern part of the Gran Paradiso massif consists of two main units, the Money Unit and the overlying Gran Paradiso Unit (Compagnoni *et al.*, 1974; Le Bayon & Ballèvre, 2006).

The Money Unit mainly consists of graphite-rich metapelites and metaconglomeratic layers intruded by the late Variscan Erfaulet granite. These rocks contain exclusively Alpine metamorphic minerals, and pre-Alpine relics are lacking (Compagnoni *et al.*, 1974) with the local exception of pre-Alpine garnet related to the contact metamorphism associated with the intrusion of the Erfaulet metagranite (Le Bayon & Ballèvre, 2004).

The Gran Paradiso Unit essentially consists of augen-gneisses derived from porphyritic granitoids of late Palaeozoic age (Bertrand *et al.*, 2000) intruded into metasediments containing lenses of basic rocks deriving either from pre-Alpine amphibolites (Compagnoni & Lombardo, 1974; Battiston *et al.*, 1984; Benciolini *et al.*, 1984; Dal Piaz & Lombardo, 1986; Ballèvre, 1988; Biino & Pognante, 1989; Brouwer *et al.*, 2002) or from late Variscan gabbros (Pognante *et al.*, 1987). The metasediments display relics of pre-Alpine layering in low-strain domains and relics of pre-Alpine metamorphic minerals in high-strain domains, namely sillimanite inclusions in muscovite porphyroclasts and pre-Alpine garnet (Callegari *et al.*, 1969; Compagnoni & Prato, 1969; Compagnoni *et al.*, 1974)

Fig. 1. Simplified structural map of the Western Alps, showing the distribution of pre-Alpine relics in continental basement units. In the external Penninic units (Ambin, Vanoise, Grand Saint Bernard), Alpine metamorphism reaches the epidote blueschist facies (Bocquet, 1974; Desmons *et al.*, 1977; Desmons, 1992; Desmons *et al.*, 1999a). In the internal Penninic Units (Monte Rosa, Gran Paradiso, and Dora-Maira), the Alpine eclogite facies event overprints pre-Alpine, amphibolite facies assemblages: two garnet generations are therefore observed in most samples preserving relics of the pre-Alpine event. The same rule holds for the Austroalpine Sesia zone, where the pre-Alpine (Permian) event reached amphibolite to granulite facies conditions (Lardeaux *et al.*, 1982; Lardeaux & Spalla, 1991; Rebay & Spalla, 2001). The various symbols (square, triangle and circle) represent the Alpine parageneses in rocks with two generations of garnet.

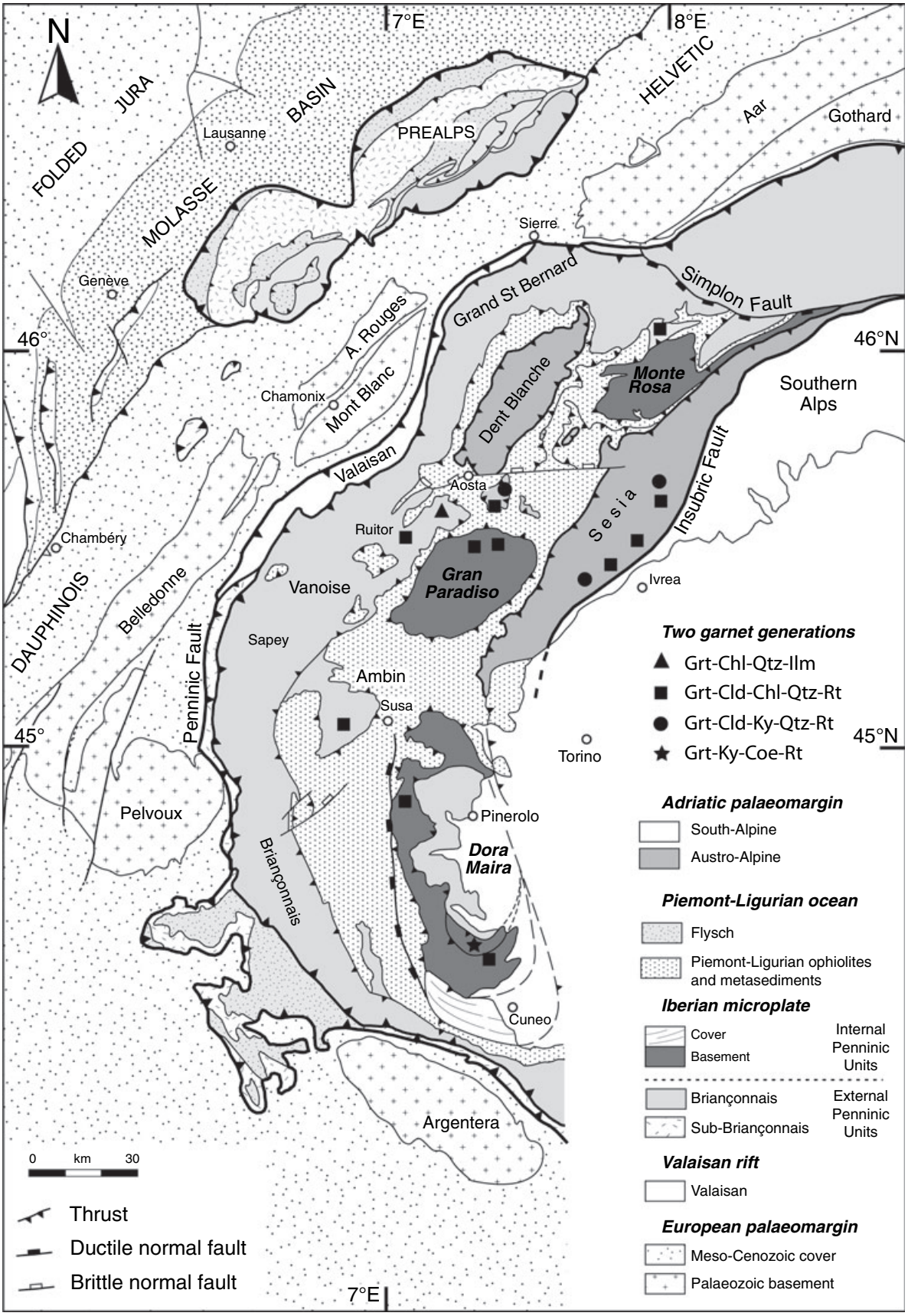

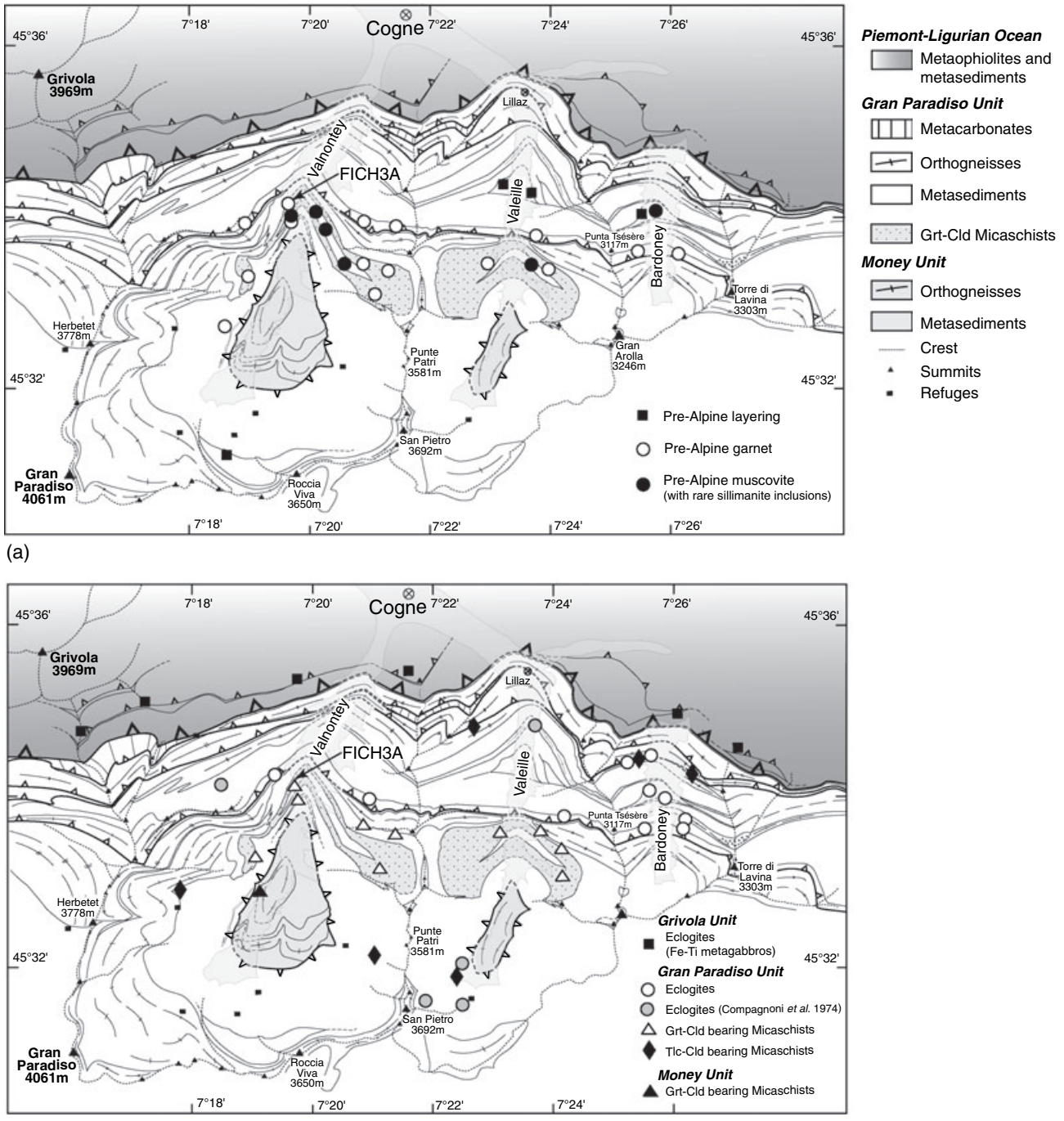

Fig. 2. Simplified geological maps of the northern part of the Gran Paradiso Massif, showing the location of the high-temperature (pre-Alpine) mineral relics (a) and the main occurrences of key high-pressure (Alpine) mineral parageneses (b). The location of the main studied sample (FICH3A; Alpe Fichelin, Valnontey valley) is also indicated. The garnet + albite-bearing 'Tsésère micaschists' are the band just above the thrust south of the Punta Tsésère.

(Fig. 2). The overprinting eclogite facies assemblages of Alpine age are identified in both the metabasic and the metasedimentary rocks of the Gran Paradiso Unit (Compagnoni & Lombardo, 1974; Chopin, 1981; Dal Piaz, 1993; Brouwer *et al.*, 2002).

Most of the *P–T* estimates in the Gran Paradiso Unit have been realized on these two lithologies. Eclogites from the Gran Paradiso Unit yielded minimum *P–T* conditions for the eclogite facies event of ~12–14 kbar, 500–550 °C (Benciolini *et al.*, 1984;

Ballèvre, 1988; Brouwer *et al*., 2002). The Al- and Mg-rich micaschists (the so-called 'whiteschists' or 'silvery micaschists') display unusual parageneses, including chloritoid, talc and phengite (Compagnoni & Lombardo, 1974; Chopin, 1981; Meffan-Main *et al*., 2004). They record eclogite facies conditions of the order of 21–23 kbar and 540–570 °C (Vidal *et al*., 2001; Wei & Powell, 2003, 2004).

The rocks re-equilibrated during decompression at ~500–550 °C, 4–6 kbar (e.g. Ballèvre, 1988; Borghi *et al*., 1996; Brouwer, 2000; Brouwer *et al*., 2002). However, some authors argue that rather than a simple decompressional recrystallization, this re-equilibration represents a late-Alpine metamorphic overprint, associated with a temperature increase, that occurred after an initial stage of cooling during decompression (Borghi *et al*., 1996; Brouwer *et al*., 2002, 2004).

MULTI-STAGE GARNET IN GRAN PARADISO

In the Gran Paradiso Unit, Borghi *et al*. (1996) argued that three garnet generations are present in the micaschists, namely a pre-Alpine, an early-Alpine (i.e. eclogitic) and a late-Alpine generation. Following a detailed study of the northern part of the Gran Paradiso massif (Le Bayon & Ballèvre, 2006) including new mapping at 1/25 000 scale, we have been able to identify two main lithologies containing multi-stage garnet.

Garnet–chloritoid-bearing micaschists have been found in two valleys (Valnontey and Valeille) in the Gran Paradiso massif (Fig. 2). These micaschists disappear towards the south, because they are affected by a kilometre-scale isoclinal fold with an east–west-trending axis (Fig. 2). At outcrop to sample scale, the garnet–chloritoid micaschists show two main phases of deformation: (i) relics of an early, microfolded schistosity (S_{A1}) best displayed at sample scale in centimetre-thick microlithons; and (ii) narrow, penetrative crenulation planes (S_{A2}) that are parallel to the axial plane of the main, kilometre-scale isoclinal fold (Fig. 3a). Locally, narrow shear bands oblique to S_{A2} are observed. In detail, the garnet–chloritoid-bearing micaschists have different appearance according to the relative amount of quartz, white mica and chloritoid. Some samples display a large amount of white mica, numerous centimetre-sized garnet (0.5–1 cm) and a few chloritoid crystals. Other samples have a higher amount of quartz compared with white mica, and they display conspicuous, centimetre-sized aggregates of chloritoid (Fig. 3b). In both types, small, millimetre-sized subhedral to euhedral garnet is present in the matrix. Bimodal distribution of garnet size and narrow overgrowths on large garnet grains suggest two stages of garnet crystallization (Fig. 4a).

A layer of garnet–albite-bearing paragneisses is mapped from the left bank of the Valnontey to the right bank of the Bardoney valley (the so-called 'Tsésère micaschists' of Borghi *et al*., 1996; Fig. 2). These paragneisses are characterized by conspicuous, centimetre-sized garnet in a matrix essentially consisting of quartz, albite, white mica, biotite, chlorite and millimetre-sized garnet. As reported by Borghi *et al*. (1996), the bimodal distribution of garnet sizes observed in most samples suggests two stages of garnet growth.

Textural relationships in the garnet–chloritoid micaschists

In order to investigate the *P–T* history of the rocks containing multi-stage garnet, several dozen samples were examined, from which a few were selected for mineral chemical analysis. The general characteristics of the garnet–chloritoid micaschists are described below, and best illustrated by the sample FICH3A (Figs 3 & 4).

First, an early foliation (S_{A1}) is defined by the alignment of quartz grains, white mica, chloritoid, elongated rutile grains (surrounded by an ilmenite rim; Fig. 4b) and rare chlorite crystals. This foliation is microfolded with various intensity and a second foliation (S_{A2}) develops in the axial plane of these folds. In places, S_{A2} is a spaced cleavage that bounds

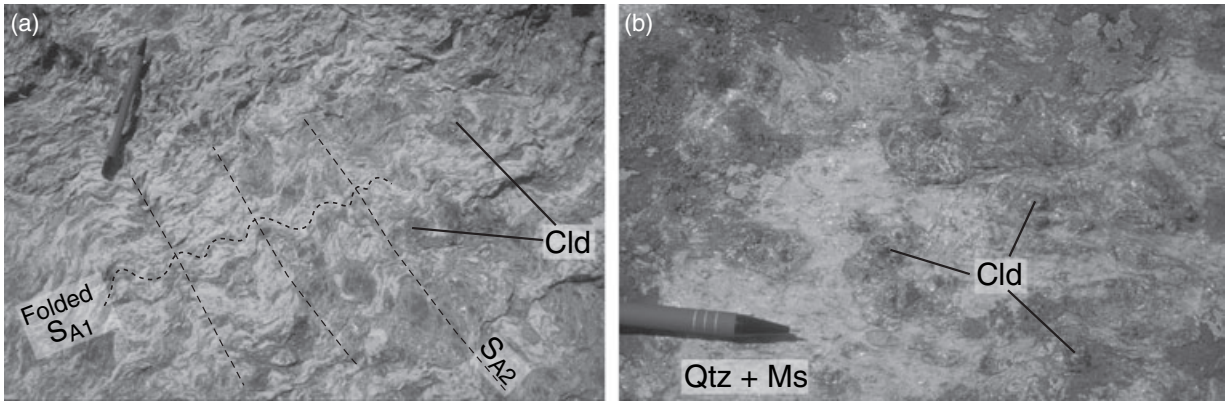

Fig. 3. Garnet–chloritoid-bearing micaschists (Pian di Ressello, Valnontey). (a) Folded schistosity (S_{A1}) in microlithons bounded by narrow foliation planes (S_{A2}); (b) centimetre-sized chloritoid aggregates in the foliation plane (S_{A2}).

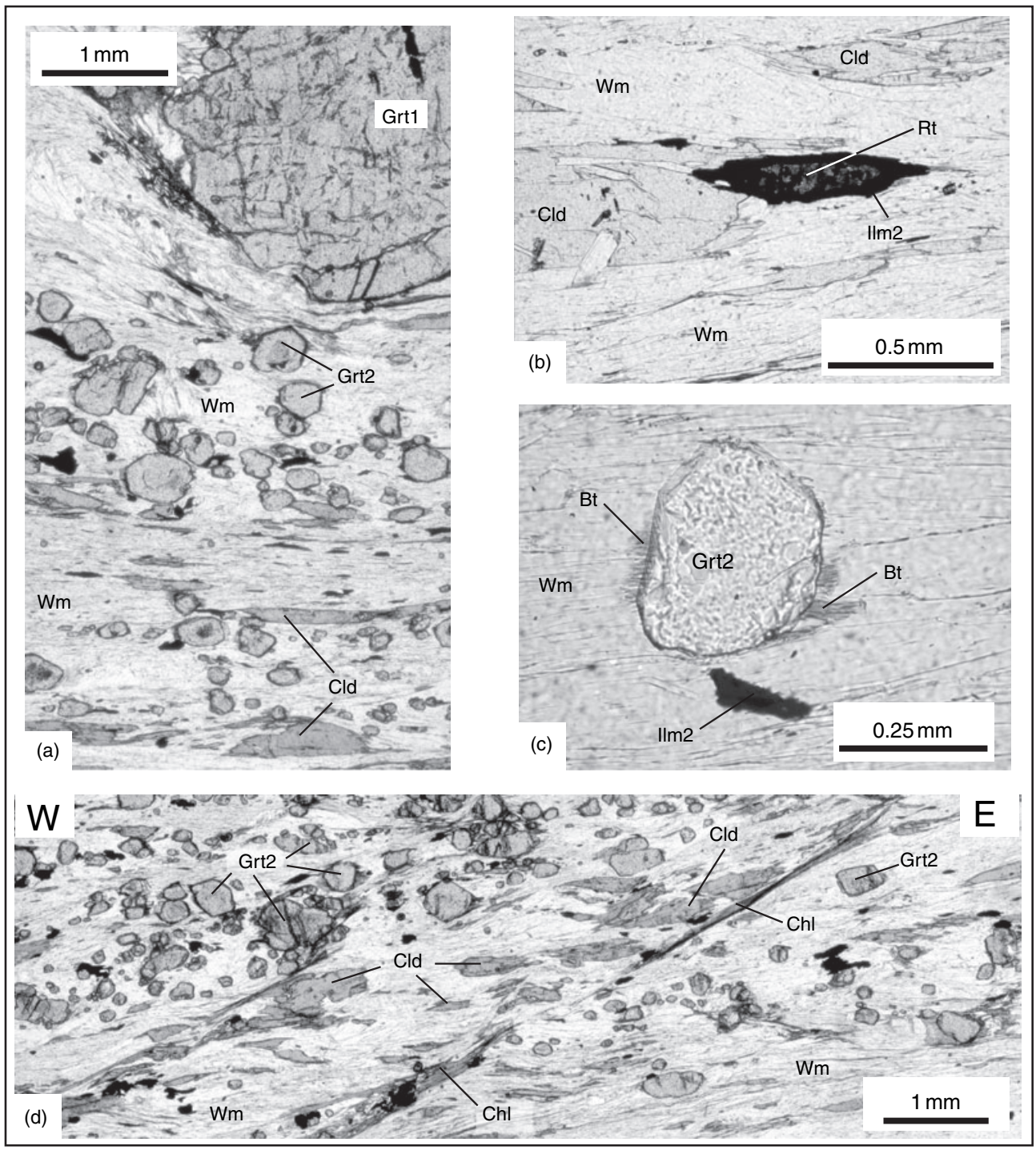

Fig. 4. Photomicrographs of sample FICH3A. (a) Two generations of garnet (garnet 1 and garnet 2) are suggested by the bimodal distribution of grain size. Because the thin section is cut parallel to the stretching lineation, S_{A1} and S_{A2} are not distinguishable. Alignment of white mica (Wm), chloritoid (Cld) and rutile (Rt) defines the foliation; (b) ilmenite (Ilm2) growth around rutile in the matrix; (c) incipient biotite growth at the contact between garnet and phengite; (d) Grt-Cld-Wm foliation deformed by late, chlorite (Chl)-bearing, shear bands.

S_{A1}-bearing microlithons (Fig. 3a), elsewhere S_{A2} entirely overprints S_{A1}. There is no mineralogical difference between the two foliations, but chlorite is more abundant where the development of S_{A2} is more intense. Chlorite is also present in the narrow shear bands cross-cutting S_{A2} (Fig. 4d).

Second, centimetre-sized oblate aggregates of chloritoid crystals (Fig. 3b) are essentially made of pale, pleochroic chloritoid containing a few rutile inclusions, and some chlorite. The chloritoid plates are elongated parallel to the early foliation S_{A1} that wraps around the aggregates, and are gently microfolded by the crenulation S_{A2}. Consequently, it may be suggested that the aggregates represent pseudomorphs after a pre-S_{A1} phase recrystallized during S_{A1}. Given the Al-rich chemical composition of chloritoid, the pseudomorphosed phase could have been staurolite. Chloritoid pseudomorphs after staurolite have indeed been found in the pre-Alpine basement of the Grand Saint Bernard area (Burri, 1983; Thélin, 1992), where the Alpine overprint is less intense compared with the studied area.

Flattened chlorite–albite aggregates of variable shape, 1–3 mm in size, are present in the matrix. Although mineralogy suggests that they may represent pseudomorphs after glaucophane, their shape is inconclusive.

Third, two types of garnet grains have been observed in these micaschists (Fig. 4a). (i) Large (0.5–1 cm) rounded garnet grains are wrapped by the mica foliation and display an inclusion-rich core and a narrow, inclusion-poor rim. Inclusions within the garnet cores consist of ilmenite, allanite, phengite and elongated, subrectangular, aggregates essentially consisting of ovoid to rounded rutile crystals and a few phengite grains. The form of the rutile–phengite aggregates and their chemical composition suggest that they may represent pseudomorphs after ilmenite. Inclusions in garnet cores are not aligned. The boundary between garnet cores and garnet rims is marked by minute quartz inclusions. Rutile inclusions are locally present in garnet rims. Unlike rutile in garnet cores, the latter forms individual prisms or needles rather than aggregates with phengite. (ii) Abundant small subhedral to euhedral garnet grains (0.05–0.5 mm) are dispersed in the matrix. They contain rare rutile inclusions and are in textural equilibrium with white mica, quartz and chloritoid in the foliation. Locally, biotite crystals grow at the garnet–phengite interface (Fig. 4c), mainly not only replacing phengite but also invading garnet, suggesting that biotite formed at the expense of both garnet and phengite.

Mineral chemistry

Chemical analyses of coexisting minerals in several samples have been performed with a Cameca SX50 electron microprobe (Microsonde Ouest, Brest, France). Operating conditions for spot analyses were 15 kV accelerating voltage, 20 nA sample current and 10 s counting time. Standards were albite (Na), orthoclase (K), corundum (Al), wollastonite (Ca, Si), forsterite (Mg), $MnTiO_3$ (Mn, Ti), Fe_2O_3 (Fe) and Cr_2O_3 (Cr). Representative mineral analyses are given in Table 1.

Table 1. Representative mineral analyses from sample FICH3A.

Mineral:	Phengite	Phengite	Phengite	Paragonite	Garnet 1	Garnet 1	Garnet 2	Garnet 2	Chloritoid	Chlorite	Ilmenite 2	Biotite	Albite
Analysis:	168	167	2	265	298	54	28	10	86	143	117	91	133
Position:	Matrix (core)	Matrix (rim)	Grt inclusion	Matrix	Core	Rim	Core	Rim	Matrix	Matrix	Matrix	Grt rim	+chl
SiO_2	50.64	47.29	50.78	47.40	36.58	35.69	36.50	36.44	24.67	24.10	0.00	34.36	69.29
TiO_2	0.24	0.13	0.81	0.10	0.01	0.07	0.03	0.00	0.00	0.04	53.41	1.59	0.00
Al_2O_3	27.05	34.23	26.12	39.03	20.98	20.61	21.26	21.21	40.66	22.21	0.06	18.41	19.25
Cr_2O_3	0.00	0.01	0.02	0.00	0.00	0.00	0.00	0.00	0.02	0.00	0.00	0.04	0.00
FeO*	2.67	1.95	2.67	0.53	33.73	38.49	32.42	36.08	24.34	30.99	45.45	21.54	0.00
MnO	0.00	0.00	0.04	0.00	3.47	1.17	1.67	0.91	0.16	0.14	0.88	0.13	0.01
MgO	3.32	1.06	3.16	0.08	1.51	2.50	1.56	2.24	2.59	10.53	0.03	7.33	0.00
CaO	0.00	0.02	0.00	0.07	3.80	1.81	6.43	3.02	0.00	0.00	0.00	0.13	0.06
Na_2O	0.26	1.07	0.24	7.04	0.02	0.05	0.00	0.02	0.02	0.02	0.00	0.14	11.57
K_2O	10.84	9.94	10.33	0.89	0.01	0.00	0.00	0.00	0.00	0.01	0.00	7.75	0.04
Total	95.02	95.69	94.17	95.13	100.10	100.37	99.87	99.92	92.47	88.05	99.83	91.43	100.22
Oxygen	22	22	22	22	24	24	24	24	6	14	3	22	32
Si	6.80	6.27	6.86	6.06	5.94	5.84	5.90	5.91	1.02	2.61	0.00	5.48	11.97
Al	4.28	5.35	4.16	5.89	4.02	3.97	4.05	4.06	1.98	2.84	0.00	3.46	3.99
Cr	0.00	0.00	0.00	0.00	0.00	0.00	0.00	0.00	0.00	0.00	0.00	0.01	0.01
Ti	0.02	0.01	0.08	0.01	0.00	0.01	0.00	0.00	0.00	0.00	1.01	0.19	0.00
Fe*	0.30	0.22	0.30	0.06	4.58	5.26	4.38	4.89	0.84	2.81	0.96	2.87	0.03
Mn	0.00	0.00	0.00	0.00	0.48	0.16	0.23	0.12	0.01	0.01	0.02	0.02	0.00
Mg	0.66	0.21	0.64	0.02	0.36	0.61	0.37	0.54	0.16	1.70	0.00	1.74	0.00
Ca	0.00	0.00	0.00	0.01	0.66	0.32	1.11	0.53	0.00	0.00	0.00	0.02	0.03
Na	0.07	0.28	0.06	1.74	0.01	0.01	0.00	0.01	0.00	0.01	0.00	0.04	3.94
K	1.86	1.68	1.78	0.14	0.00	0.00	0.00	0.00	0.00	0.00	0.00	1.58	0.03
Total	14.00	14.02	13.89	13.93	16.00	16.18	16.06	16.06	4.00	9.97	1.99	15.41	20.01
X_{Fe}	0.31	0.51	0.32	0.78	0.93	0.90	0.92	0.90	0.84	0.62		0.62	
X_{Na}/X_{An}	0.04	0.14	0.03	0.92									0.01
Alm					0.75	0.83	0.72	0.80					
Sps					0.08	0.03	0.04	0.02					
Prp					0.06	0.10	0.06	0.09					
Grs					0.11	0.05	0.18	0.09					

*All Fe is assumed to be divalent.

Garnet

Both types of garnet are almandine-rich and strongly zoned. However, differences in the zoning pattern allow an unequivocal distinction between the two types. X-ray element maps for Ca, Mn, Mg, Fe and Ti realized on several garnet crystals in several samples and best illustrated in the garnet–chloritoid micaschist sample FICH3A (Fig. 5a) show that: (i) the optical discontinuity in large garnet porphyroblasts between core (garnet 1) and rim overgrowths (garnet 2) coincides with a strong chemical discontinuity; and (ii) the small garnet crystals in the matrix have the same composition as the narrow overgrowths around the larger grains, corresponding therefore both to the same garnet generation (garnet 2).

Chemical zoning in garnet 1 (Fig. 5b) is characterized by a core-to-rim decrease in grossular (from 11 to 4–5 mol.%) and spessartine contents (from 8–10 to 3 mol.%) compensated by an increase in the contents of almandine (from 70–75 to 83 mol.%) and pyrope (from 4–6 to 10 mol.%). X_{Fe} [= Fe/(Fe + Mg)] decreases smoothly from 0.94 to 0.89 (locally as low as 0.85).

Chemical zoning is also observed in garnet 2 (Fig. 5b, c). The innermost part of garnet 2 (Grt2a) is characterized by a slight increase in grossular content (from 15 to 18–20 mol.%) and a decrease of the X_{Fe} ratio (from 0.93 to 0.92). The transition towards the outer part of garnet 2 is marked by a narrow zone (~20 μm) of strong but continuous decrease of X_{Fe} and the grossular content. The outer part of garnet 2 (Grt2b) is characterized by a low grossular content (8 mol.%) and a low X_{Fe} ratio (0.90). The spessartine content decreases smoothly from the core to the rim (from a maximum of 8 to 2 mol.%).

The transition from garnet 1 rims to the garnet 2 overgrowths is therefore marked by a sharp compositional discontinuity, best exemplified by the jump in grossular content from 4–5 to 15 mol.% (Fig. 5). Figure 5b,c also documents the differences in diffusional behaviour between different elements across the boundary of garnet 1 and 2. Virtually no exchange is observed for Ca, but Mn and X_{Fe} display a re-equilibration across ~50 μm. In agreement with other studies (Hiroi & Ellis, 1994; Lanzirotti, 1995; Spear & Kohn, 1996), this implies that whereas the grossular content of garnet is a robust and reliable indicator of the metamorphic evolution, the X_{Fe} ratio and especially the spessartine content are more easily re-equilibrated and therefore less useful for quantitatively identifying *P–T* conditions.

Furthermore, X-ray element maps for garnet 1 have revealed the occurrence of domains with compositions similar to those of the inner part of garnet 2 (Figs 5 & 6). Such domains occur in two situations.

First, they define narrow, linear zones that end up at the boundary with garnet 2 (Fig. 6). Optically, these linear domains are only barely identifiable, except for the alignment of a few minute inclusions (mostly tiny white mica). They are interpreted as former fractures that cut across garnet 1, and were sealed during the growth of garnet 2. Garnet composition in these frac-

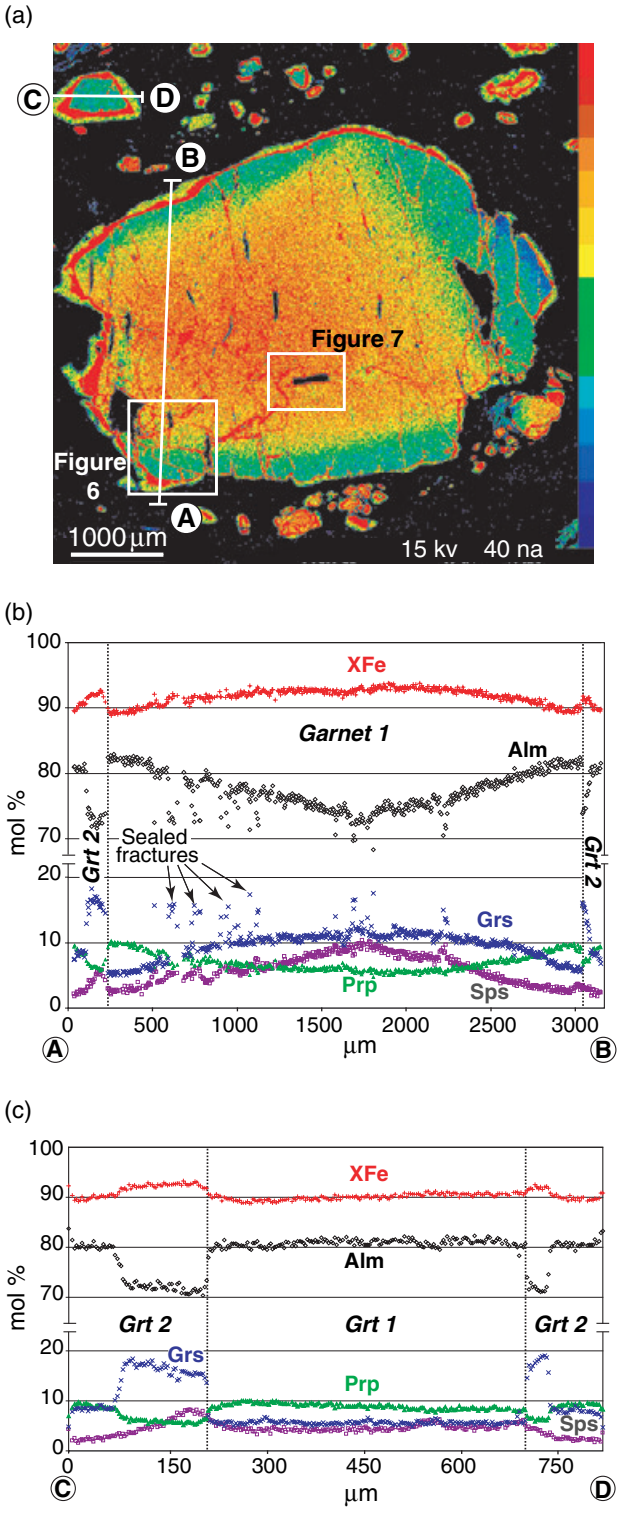

Fig. 5. Chemical composition of a large garnet in sample FICH3A. X-ray element map for Ca (a) and chemical zoning profile along a north–south line through the garnet core (b).

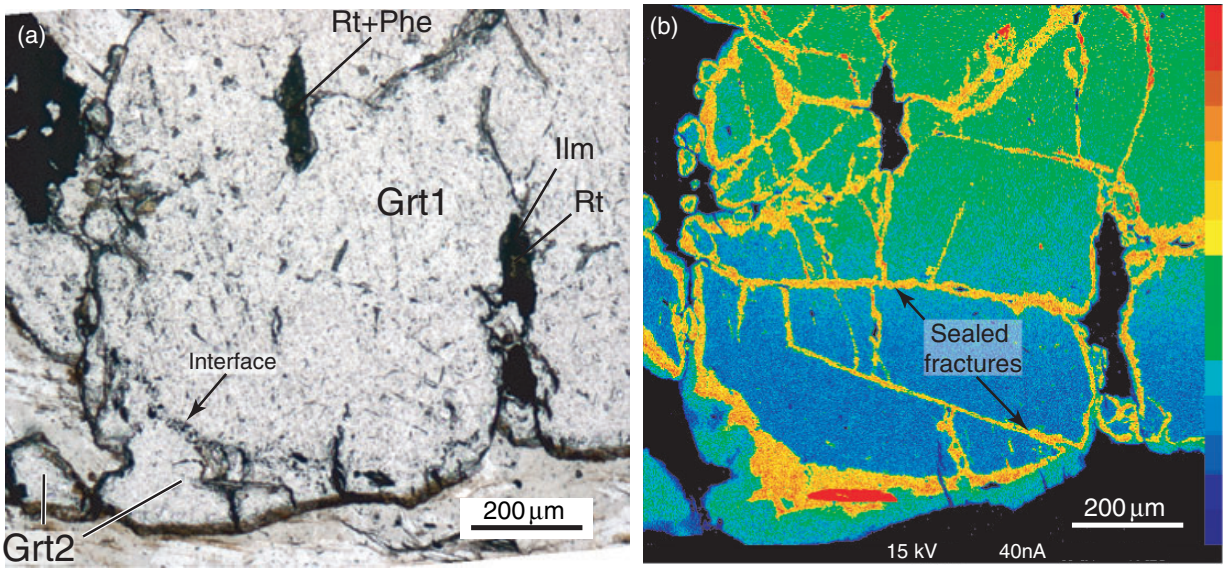

Fig. 6. Detail of the garnet rim from Fig. 5. (a) Photomicrograph, (b) Ca X-ray map revealing the presence of sealed fractures.

tures is the same as that of the inner part of garnet 2 (especially for the high Grs content). These sealed fractures imaged by the X-ray maps indicate that garnet 1 experienced brittle deformation before the new stage of growth.

Second, aggregates of rutile and phengite in garnet cores are surrounded by a narrow, grossular-rich domain (Fig. 7), the composition of which is similar to the Grs-rich garnet 2. This domain was connected via the now sealed fractures to the matrix, as revealed by X-ray element maps. Ilmenite inclusions found in garnet cores and unaffected by the fractures are not surrounded by such a Ca-rich domain. It is therefore thought that the rutile–phengite aggregates derive from former ilmenite inclusions that have been re-equilibrated in an open system because of former connections with the matrix.

Other minerals

Chemical composition of chloritoid is homogeneous [$X_{Fe} = 0.80–0.85$; $X_{Mn} = Mn/(Mn + Fe + Mg) = 0.009–0.01$], and the crystals do not display chemical zoning. Chlorite in the matrix displays a relatively homogeneous chemical composition ($X_{Fe} = 0.57–0.59$; $X_{Al,T2} = 0.64–0.68$; $X_{Mn} = 0.001–0.004$). Chlorite in

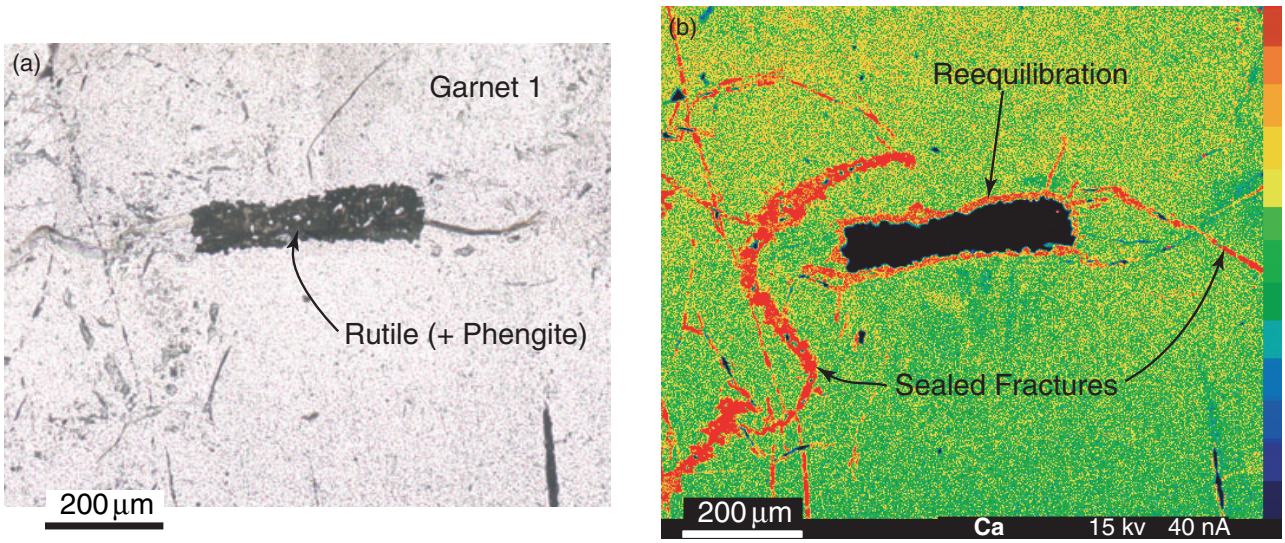

Fig. 7. Detail of the garnet core from Fig. 5, surrounding a subrectangular rutile (+phengite) aggregate. (a) Microphotograph, (b) Ca X-ray map revealing the presence of a Ca-rich zone at the contact between the former inclusion and the garnet host.

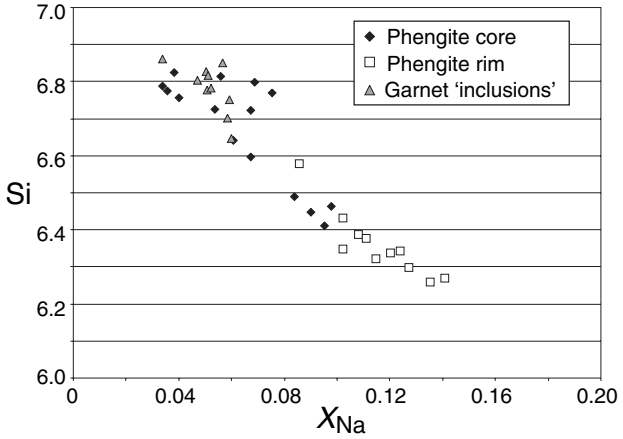

Fig. 8. Muscovite composition. A negative correlation exists between the Si-content (apfu) and the X_{Na} (= Na/Na + K) ratio of muscovite. Cores of the crystals are systematically more Si-rich and Na-poor. Muscovite recrystallized in re-equilibrated inclusions of garnet 1 (garnet inclusions) have the same composition as the cores of matrix crystals.

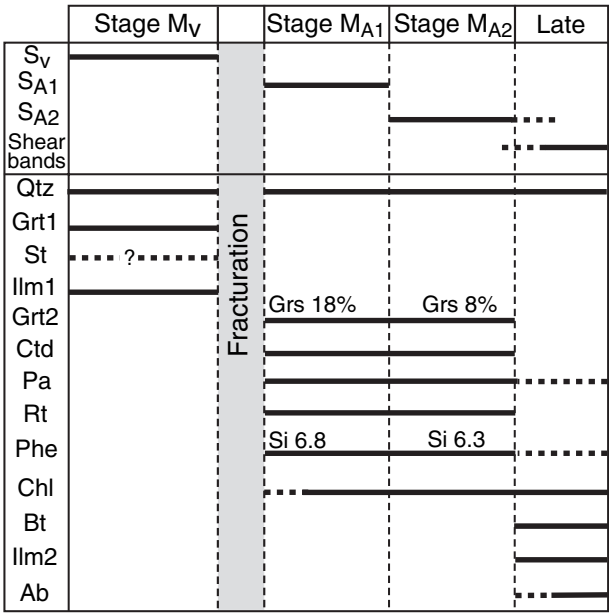

Fig. 9. Paragenetic sequence in sample FICH3A deduced from microtextural observations and microchemical analyses.

pressure shadows around garnet is more ferrous and aluminous ($X_{Fe} = 0.62$; $X_{Al,T2} = 0.70$; $X_{Mn} = 0.003$).

Two types of white mica are present in the sample. Matrix paragonite has a high Na content [X_{Na} = Na/(Na + K) = 0.89–0.96] and a low Ca content [X_{Ca} = Ca/(Ca + Na + K) = 0.001–0.006]. Paragonite inclusions in garnet have a higher X_{Ca} (0.014). Muscovite is phengitic and displays chemical zoning (Fig. 8) with a decreasing amount of phengite substitution and an increase in both X_{Na} and X_{Fe} from core (Si = 6.60–6.84 apfu; $X_{Na} = 0.04$–0.10; $X_{Fe} = 0.30$–0.45) to rim (Si = 6.26–6.42 apfu; $X_{Na} = 0.13$–0.17; $X_{Fe} = 0.50$–0.56). Minute phengite inclusions in garnet 1 are located either along sealed fractures or in rutile aggregates. In both cases, the inclusions have a high Si content (Si = 6.65–6.86 apfu), their composition being similar to the cores of matrix grains.

Ilmenite is present both in garnet 1 cores and in the matrix. However, the chemical composition is homogeneous and independent of the textural position, characterized by only limited amounts of the pyrophanite component (2 mol.%). Plagioclase is almost pure albite ($X_{An} < 0.01$).

To sum up, two metamorphic events can be distinguished in the garnet–chloritoid micaschists (Fig. 9). The first event is recorded by the cores of large garnet (garnet 1). Inclusions of ilmenite (ilmenite 1) are the only relic of the associated paragenesis (stage M_V). Staurolite now replaced by chloritoid aggregates might have been a member of this paragenesis. Metamorphic evolution during this first metamorphic event is recorded in growth zoning of garnet 1.

The second metamorphic event is recorded by the crystallization of garnet 2 that overgrows garnet 1. The early stage of this process is contemporaneous with open-system re-equilibration of event 1 inclusions and then sealing of garnet 1 fractures. This second metamorphic event (M_A) is characterized by the assemblage garnet + chloritoid + phengite + paragonite ± chlorite + quartz + rutile. Chemical zoning of garnet 2 and the decrease of the phengite substitution in muscovite records the metamorphic evolution during this event. Biotite growth at the expense of garnet and phengite, replacement of matrix rutile by ilmenite (ilmenite 2), and chlorite development in the shear bands characterize the late metamorphic evolution of the micaschists.

NUMERICAL MODELLING OF MINERAL ASSEMBLAGES

P–T pseudosections were calculated with THERMOCALC v. 3.25 (Powell & Holland, 1988) and the internally consistent thermodynamic dataset 5.5 (Holland & Powell, 1998: November 2003 upgrade) with two main objectives: (1) to evaluate the record of the *P–T* history of the micaschists provided by the multi-stage garnet; and (2) to estimate the *P–T* conditions of the two metamorphic stages. Two *P–T* pseudosections were calculated in the model system MnNCKFMASH and contoured with compositional isopleths of garnet and muscovite. The bulk-rock compositions were calculated using the modal proportions (determined by point counting) and chemical compositions of the minerals present. Equilibration at the scale of the thin section was assumed for the early metamorphic evolution of the sample (FICH3A) – explored in the first pseudosection (Fig. 10). On the other hand, cores of large garnet are known to strongly fractionate some components and thereby modify the effective bulk

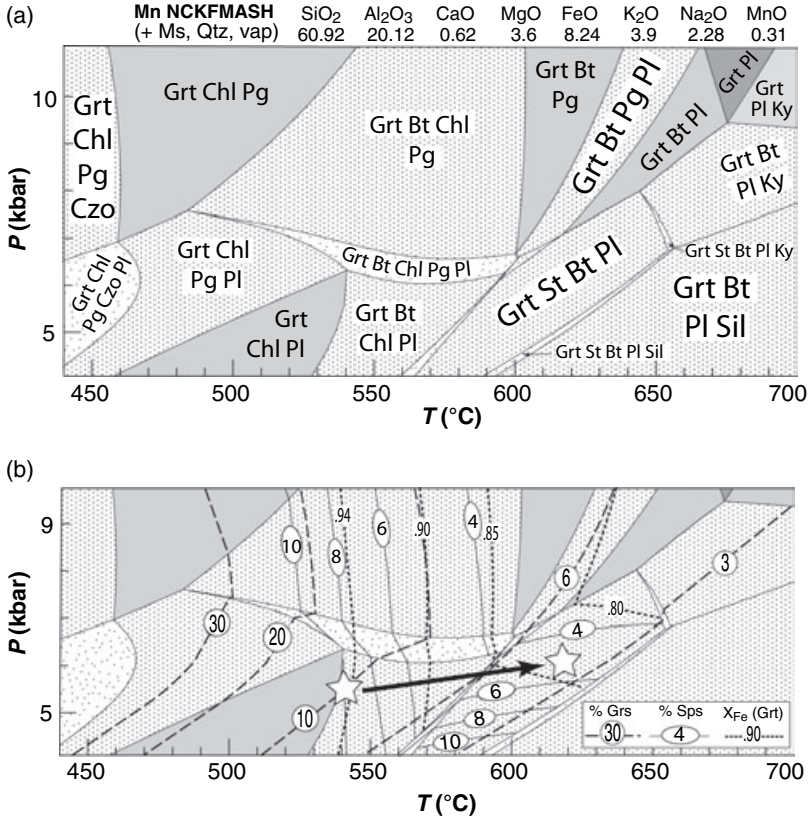

Fig. 10. Calculated *P–T* pseudosection for sample FICH3A contoured with compositional isopleths of garnet [X_{Fe} (= Fe/(Fe + Mg) and mol.% of grossular and spessartine] in order to interpret the zoning recorded by garnet 1.The bulk composition (in mol.%) was determined from the mode and chemical compositions of the minerals, assuming equilibration at the scale of the thin section.

composition available for later recrystallization. Consequently, only the matrix phases, small matrix garnet and the rims of large garnet (i.e. garnet 2) were assumed in equilibrium and their mode used for calculation of the effective bulk-rock composition in the second pseudosection (Fig. 11) used to constrain the metamorphic evolution of the sample after the crystallization of garnet 1, during the second event. Finally, as the amount of available H_2O has a strong influence on the retrograde paragenetic evolution of rocks (e.g. Guiraud *et al.*, 2001; Proyer, 2003), a pseudosection with a fixed amount of H_2O was calculated in order to discuss the late evolution of the studied sample (Fig. 12).

P–T conditions during garnet 1 growth

As a result of the lack of suitable inclusions in the cores of large garnet, the preserved chemical zoning and the possible pseudomorphs after staurolite are the only indicators of the *P–T* evolution of the sample during the first metamorphic stage (Fig. 10). The composition of the garnet cores ($X_{Fe} = 0.94$, Grs = 0.11, Sps = 0.09) implies that they equilibrated in the Grt-Chl-Bt-Pl field, at ~5–6 kbar, 540 °C, where the corresponding isopleths intersect (Fig. 10). The systematic rimward decrease in X_{Fe} and in the proportions of Grs and Sps components reflects a temperature increase. Garnet 1 rims ($X_{Fe} = 0.85$, Grs = 4–5%, Sps = 2–4%) equilibrated at ~620 °C, 6 kbar, in the Grt-St-Bt-Pl stability field (Fig. 10b). This supports the hypothesis that the chloritoid aggregates indeed represent deformed pseudomorphs after staurolite. Under these *P–T* conditions, the calculated content of spessartine (4–6%) is higher than that measured in garnet 1 rims. This results from the fact that progressive fractionation of Mn into the crystallizing garnet has not been taken into account. However, this has only a negligible effect on the other compositional variables.

P–T conditions during garnet 2 growth

The second metamorphic assemblage consists of garnet 2, chloritoid, paragonite, phengitic muscovite, quartz, rutile and rare chlorite. In the calculated pseudosection (Fig. 11), the corresponding Grt-Cld-Pg-Chl (+Ms-Qtz) stability field spans 11–20 kbar and 460–580 °C (Fig. 11). Because muscovite displays distinct chemical zoning ($Si_{core} = 6.6$–6.8 apfu, $Si_{rim} = 6.3$–6.4 apfu), the pseudosection was also contoured for the amount of Si in muscovite. Si(Ms) isopleths displaying a slightly positive slope in the Grt-Cld-Chl-Pg stability field allow good pressure estimation during the second metamorphic event, yielding a minimum pressure of 18 kbar for the crystallization of the muscovite cores. Taking into account the chemical composition of the outer part of garnet 2 cores ($X_{Fe} = 0.92$–0.93, Grs = 18–20%), *P–T* conditions of ~490 °C at 18–20 kbar

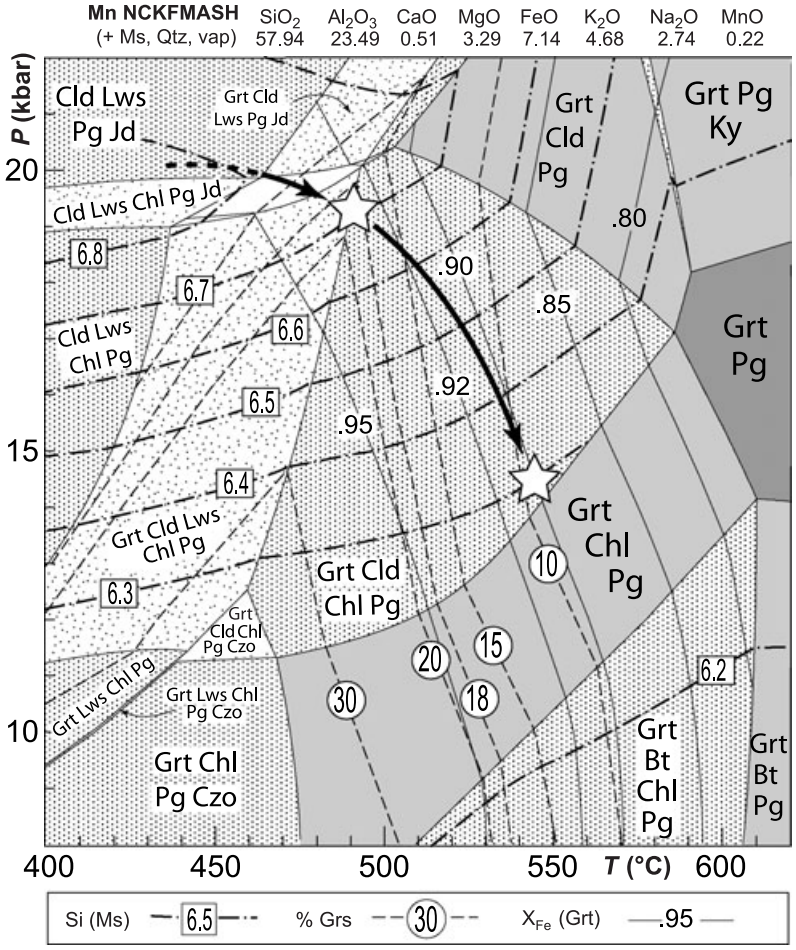

Fig. 11. Calculated *P–T* pseudosection for sample FICH3A, for a bulk composition determined assuming that only the matrix phases and the rims of large garnet (i.e. garnet 2) were in equilibrium. Glaucophane was not considered in the calculations (cf. Fig. 13). Garnet being the only Ca-bearing phase in the Grt-Cld-Chl-Pg field, the isopleths of the grossular content (% Grs) are parallel to the isopleths of garnet mode, which increases with increasing temperature (cf. Fig. 12). The orientation of the isopleths reveals that garnet can only grow on decompression if heating is involved. The composition of muscovite cores is more successfully reproduced in the Grt-absent Cld-Lws-Pg ± Chl ± Jd fields. Open stars are *P–T* conditions deduced from the intersection of the appropriate compositional isopleths. Accordingly, the sample recorded decompression accompanied by moderate heating.

can be suggested for the formation of the Grt2a-Cld-Chl-Pg (+Ms-Qtz) paragenesis (Fig. 11). Table 2 documents that there is indeed a good agreement between the observed and modelled modes and chemical compositions of these phases. These *P–T* conditions also correspond to the conditions at which the sealing of garnet 1 fractures was accomplished. Nonetheless, the highest Si contents measured in the muscovite cores and muscovite 'inclusions' in garnet are not modelled in the pseudosection in the Grt-Cld-Pg-Chl field. These values (Si > 6.8 apfu) require equilibration at lower temperatures, in the Grt-absent Cld-Lws-Pg ± Chl ± Jd fields. Indeed, strictly speaking, there is no evidence that muscovite cores and 'inclusions' equilibrated with the garnet–chloritoid–chlorite–paragonite paragenesis and their compositional range may reflect a portion of the *P–T* path dominated by heating close to the pressure peak. Additionally, such a *P–T* evolution is in agreement with the observed increase of the grossular content in the cores of garnet 2.

The rim of garnet 2 (Grt2b) is also in equilibrium with white mica, chloritoid, quartz and rare chlorite. The composition of garnet 2 rims ($X_{Fe} = 0.90$, Grs = 8–10 mol.%) and muscovite growth zoning (Si decreasing to 6.4–6.3 apfu) suggest decompression accompanied by moderate heating in the Grt-Cld-Pg-Chl field to ~14–15 kbar, 540–550 °C (Fig. 11, Table 2). During this evolution, the mol.% of garnet and chlorite increases at the expense of chloritoid and paragonite. Muscovite becomes less phengitic and more sodic and there is again a good correlation between the measured and calculated mineral compositions (Table 2).

Late *P–T* evolution

Local crystallization of biotite at the garnet–phengite interface (Fig. 4c) suggests further decompression and equilibration in biotite-bearing fields. Furthermore, it is infered from the observed garnet resorption during this stage, and the modelled slightly negative slope of the isopleths of garnet mol.% (Fig. 12), that this decompression was not accompanied by substantial heating. On the contrary, we believe that cooling is compatible with the very localized and incomplete record of this *P–T* stage. As availability of H_2O is essential for reaction during a *P–T* evolution involving cooling (e.g. Guiraud *et al.*, 2001; Proyer, 2003), the

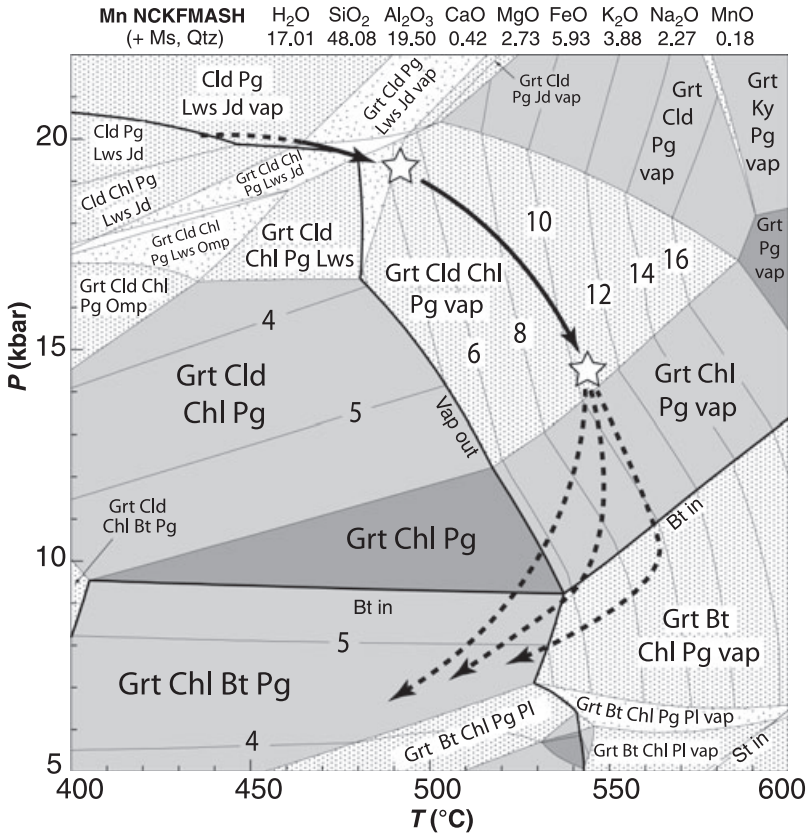

Fig. 12. *P–T* pseudosection calculated for the bulk composition used in Fig. 11 with H_2O fluid (vap) not considered in excess. The amount of H_2O in the bulk composition was estimated so that at peak temperature, inferred from Fig. 11, the amount of free fluid phase in the rock did not exceed 2 mol.%. Compared to Fig. 11, water undersaturation results in the absence of lawsonite and clinozoisite and stabilization of biotite at low temperatures. Furthermore, the position of garnet-mode isopleths suggests that only limited garnet resorption results from cooling under water undersaturated conditions. The three dashed lines represent the possible retrograde *P–T* paths.

Table 2. Summary of measured modes (%) and calculated mol.% and selected compositional variables of phases crystallized during the second metamorphic event (M_{A1}–M_{A2}).

P–T stage		Measured			Calculated 19.5 kbar–492 °C (M_{A1})		Calculated 14.5 kbar–545 °C (M_{A2})	
Phase	Variable	Mode	Core	rim/mx	Mode	Compo.	Mode	Compo.
Grt	X_{Fe}	9.8	0.92	0.90	5.4	0.93	10.6	0.90
	X_{Grs}		0.18	0.08		0.18		0.09
	X_{Sps}		0.06	0.02		0.07		0.04
Cld	X_{Fe}	4.9		0.80–0.85	12.3	0.83	0.8	0.80
	X_{Mn}			0.01		0.01		0.00
Chl	X_{Fe}	2.2		0.57	2.4	0.51	8.4	0.50
	y			0.67		0.51		0.53
Ms	X_{Fe}	52.8	0.30–0.45	0.50–0.56	52.1	0.45	54.3	0.48
	Si(apfu)		6.60–6.80	6.26–6.42		6.72		6.30
	X_{Na}		0.04–0.10	0.13–0.17		0.06		0.14
Pg	X_{Na}	27.2		0.89–0.96	24.6	0.99	20.8	0.96
Qtz		1.6			2.3		3.2	
H2O					0.9		1.9	

Chlorite – y = X(Al,T2) = (4 – Si)/2; $X_{Mn} < 0.01$.

P–T pseudosection of Fig. 11 was recalculated with a fixed amount of H_2O (Fig. 12). This amount was estimated so that at peak temperature (inferred from Fig. 11), the proportion of free fluid phase in the rock did not exceed 2 mol.%. Compared with Fig. 11, water undersaturation results in the absence of lawsonite and clinozoisite and stabilization of biotite at low temperatures. Furthermore, the position of garnet mol.% isopleths suggests that only limited garnet resorption results from cooling under water-undersaturated conditions. Moreover, a *P–T* evolution involving cooling would rapidly result in fluid-absent conditions, making complete recrystallization of the rock difficult, which is in agreement with the observations. Unfortunately, the local character of recrystallization also implies very small volumes of equilibration. Consequently, the pseudosection calculated for a global bulk composition (albeit without garnet 1) cannot be used rigorously

(e.g. for comparing the calculated and measured compositions of late chlorite and biotite or understanding the local development of chlorite–plagioclase aggregates) and can only yield qualitative insights into the late stages of metamorphic evolution.

DISCUSSION

Role of glaucophane

The possibility that glaucophane was present in the garnet–chloritoid micaschists cannot be discounted, although conclusive evidence has not been found despite the local presence of chlorite–albite aggregates. However, the position of the glaucophane-in equilibria in the calculated *P–T* pseudosections depends strongly on the solid–solution model used (Fig. 13).

Using the model of Wei *et al.* (2003), glaucophane appears by virtue of narrow di- and trivariant fields equivalent to the subisobaric NCKFMASH reaction Grt + Chl = Gln + Cld (+Ms, Pg, Lws/Zo, Qtz, H_2O) at ~18 kbar (Fig. 13a). This reaction controls the development of glaucophane in most aluminous pelitic lithologies, including sample FICH3A, projecting between chloritoid and the Grt-Chl joint in the AFM-type diagram (cf. fig. 5 in Wei & Powell, 2006). Consequently, moderate variations in bulk composition could not explain the absence of glaucophane at pressures above this reaction. According to the position of the compositional isopleths, muscovite and garnet 2 cores would have equilibrated in the Grt-Cld-Pg-Gln field at *P–T* conditions identical to those inferred from Fig. 11 – about 18–20 kbar, 490–500 °C. The small amount of glaucophane present at this stage (~5 mol.%) could have easily reacted out during subsequent evolution, identical again to that deduced from Fig. 11.

On the other hand, if glaucophane is modelled using the thermodynamic model of Dale *et al.* (2005), the NCKFMASH reaction Grt + Chl = Gln + Cld (+Ms, Pg, Lws/Zo, Qtz, H_2O) has a strongly positive slope (10 kbar at 440 °C, 18 kbar at 550 °C) and the stability of glaucophane expands considerably towards low pressures (Fig. 13b). In consequence, the stability field of the main observed paragenesis Grt-Cld-Chl-Pg shrinks to merely a narrow band just beyond the Gln-in line. Moreover, the isopleths of Si(Ms) are shifted towards high pressures and there is no intersection between the isopleths corresponding to the composition of the cores of muscovite and garnet 2. Additionally, the highest values of Si-content measured in the muscovite cores and muscovite 'inclusions' in garnet are modelled in the pseudosection only at extremely high pressures or low temperatures. In consequence, it is difficult to interpret the observed equilibrium relations in the framework of this diagram.

The presence of glaucophane in our samples is uncertain and we believe that investigating the validity

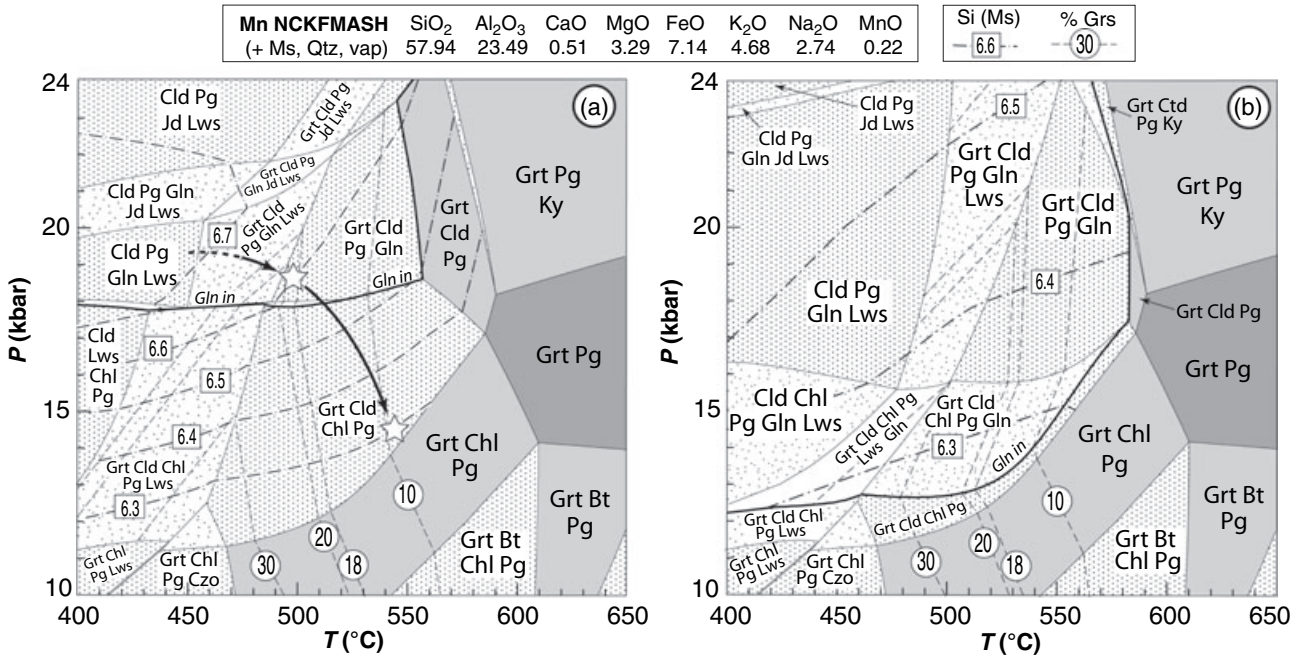

Fig. 13. *P–T* pseudosections from Fig. 11 recalculated for glaucophane-bearing equilibria using the glaucophane mixing model of (a) Wei *et al.* (2003) and (b) Dale *et al.* (2005) and contoured with compositional isopleths. Using the model of Wei *et al.* (2003), the inferred *P–T* evolution is identical to that of Fig. 11 (a). On the other hand, the new model strongly extends the glaucophane stability field and results in a topology and position of the compositional isopleths incompatible with our observations (b). See text for more detail.

of various glaucophane models is beyond the scope of this work. Figure 11 represents the possible case where glaucophane-bearing equilibria appear only above 22 kbar. Nevertheless, Fig. 13a yields an identical *P–T* evolution.

P–T evolution recorded by multi-stage garnet

Summarizing the data provided by the textural analysis, the chemical composition of coexisting phases, and the numerical modelling allows the following scenario to be proposed (Fig. 14).

Garnet 1 and ilmenite are the only relics of a first metamorphic stage, occurring at intermediate pressure and relatively high temperature (5–7 kbar and 600–650 °C). The zoning profile in garnet 1 preserved part of the *P–T* evolution during this stage (a temperature increase of ~70–100 °C). This high temperature stage is attributed to a pre-Alpine (Variscan) event (M_V). These inferred *P–T* conditions are located close to the Ky-Sil transition in *P–T* space. Subsequent decompression, possibly accompanied by moderate heating is compatible with the observed presence of sillimanite in other lithologies. No other estimation of the *P–T* conditions of the pre-Alpine event is available in Gran Paradiso. However, this result is compatible with those obtained in other Penninic units, like the Mont Mort area in the Grand Saint Bernard nappe (Thélin, 1992) or in the Ambin massif (Ganne *et al.*, 2003).

The second metamorphic event, occurred at relatively high pressure (~18–20 kbar and 490 °C). A second stage of garnet growth (garnet 2) took place, producing either overgrowths on pre-existing grains, or new crystals in the matrix, in equilibrium with chloritoid, chlorite, paragonite, phengite and rutile. Because of the high pressures attained, this event is attributed to the continental subduction of early-Alpine age (M_{A1}). Estimates of the *P–T* conditions for the eclogite

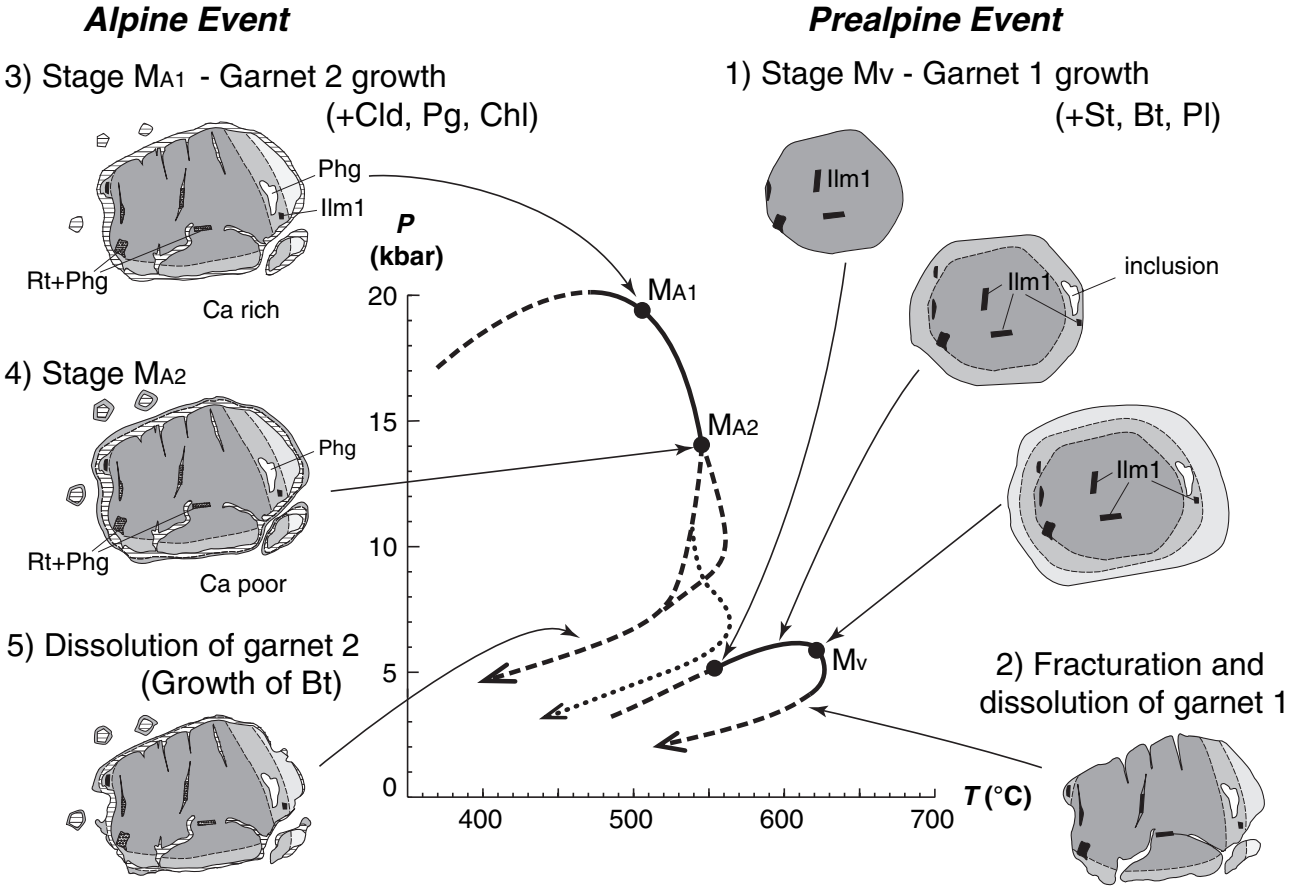

Fig. 14. Schematic diagram showing the evolution of the multi-stage garnet from the Gran Paradiso garnet–chloritoid micaschists. Garnet 1 records initial prograde growth during the pre-Alpine (Variscan) history, followed by partial dissolution and fracturing (possibly during exhumation of the Variscan rocks). Garnet 2 represents a new stage of growth, which developed during subduction/exhumation of the European continental crust in the convergent zone between Adria and Europe. Fractures are healed with garnet 2 and most inclusions are pseudomorphed by new minerals. Exhumation of the subducted crust has been accompanied by continued garnet growth at slightly increasing temperature. Further exhumation, accompanied by cooling, resulted in limited garnet resorption and local crystallization of biotite. The portion of the *P–T* path involving late heating at low pressures, proposed by Brouwer *et al.* (2002), is indicated as a dotted line for comparison.

facies event in the Gran Paradiso massif are not wholly consistent with our calculations. The results obtained by Brouwer *et al.* (2002) suggest significantly lower pressures with respect to our results. However, this arises from the fact that the method used by these authors (Jd-Qtz-Ab geobarometry) is only able to yield minimum pressure estimates in eclogites. Using the whiteschists, Wei & Powell (2003, 2004), based on previous studies by Chopin (1981), calculated higher peak pressures (of the order of 21–23 kbar). However, those samples were collected in the region of Bonneval, in the south-westernmost part of the Gran Paradiso massif, more than 30 km from our sample. Consequently, the difference with our results probably reflects the existence of a metamorphic field gradient in the Gran Paradiso massif. Indeed, significant *P–T* gradients are known to exist in other eclogite facies units (e.g. Heinrich, 1986; Dale & Holland, 2003).

Continued garnet growth is recorded by the zoning profile of garnet 2, and the calculated pseudosection indicates that the zoning records decompression at slightly increasing temperature to ~14–15 kbar, 540–550 °C (M_{A2}). Further decompression and cooling led to the development of lower pressure parageneses, including biotite, chlorite, paragonite, Si-poor muscovite, ilmenite and locally albite. However, because of incomplete re-equilibration, the shape of the *P–T* path during this stage is poorly constrained. The narrow, chlorite-bearing shear bands that represent the latest increments of strain at the end of the ductile deformation of the studied samples developed during these waning stages of the metamorphic history.

Two or three garnet generations?

The occurrence of multi-stage garnet has already been described in the European continental basement from the Western Alps (Fig. 1). In general, two garnet generations have been recognized, namely a pre-Alpine garnet (as large, relic grains), and an Alpine garnet (as overgrowths or as small euhedral crystals). Locally, however, three garnet generations have been described in metapelites from the Dora-Maira massif (Borghi *et al.*, 1985; Sandrone & Borghi, 1992) and the Gran Paradiso massif (Borghi *et al.*, 1996): they were ascribed to a pre-Alpine stage, an early-Alpine (high pressure) and a late-Alpine (low pressure) stage, respectively. Based on the interpretations of Borghi *et al.* (1996), Brouwer *et al.* (2002) argued for a late thermal pulse related to mantle delamination during the late-Alpine tectonic evolution.

In this study, we have shown that large garnet grains (garnet 1) are the main relics of the pre-Alpine metamorphic event, occurring at relatively low pressure and high temperature. The low temperatures estimated for the Alpine metamorphism (max. 500–550 °C) and the short duration of the Alpine high-pressure stage (cf. Rubatto & Hermann, 2001) may have prevented diffusive re-equilibration of the pre-Alpine garnet. Therefore, garnet 1 preserves its growth zoning and displays features related to its partial dissolution before the growth of garnet 2, and even fractures sealed by garnet 2. Fractures and dissolution may have been accompanied by partial replacement of pre-Alpine garnet by chlorite and/or biotite, as described in the Ruitor and Grand Saint Bernard area (Burri, 1983; Thélin, 1992). In these areas, the Alpine overprint occurred at lower *P–T* conditions compared with Gran Paradiso, and the pre-Alpine fractures were not sealed during a second stage of garnet growth. The occurrence of sealed fractures in garnet has been observed in other eclogite facies rocks, for example, in Proterozoic granulites reworked during the Caledonian orogeny (Erambert & Austrheim, 1993; Engvik *et al.*, 2000). Re-equilibration of inclusions has also been described in garnet from medium- to high-grade rocks (Whitney, 1991), and has been reproduced experimentally (Perchuk *et al.*, 2005). In both cases, the processes involved some elemental exchange with the matrix.

Garnet 2 is characterized by a slightly zoned grossular-rich (15–20%) core and a homogeneous grossular-poor (8%) rim. This pattern suggests that the rims of garnet 2 represent a third generation of garnet growth. However, careful observation of the narrow transitional zone between garnet 2 cores and rims reveals a strong but continuous decrease of the grossular content (Fig. 5c), unlike the truly discontinuous transition between garnet 1 and garnet 2. No evidence of garnet resorption is documented within garnet 2. Accordingly, it is clear that only one generation of garnet crystallized continuously during the second, Alpine metamorphic event. The *P–T* evolution proposed for this event in Fig. 11 would produce a smooth core-to-rim decrease in grossular, rather than the 'step-like' zoning pattern observed. However, as garnet is the only Ca-bearing phase in the Grt-Cld-Chl-Pg field (Fig. 11), garnet mol.% is directly related to the grossular content. Consequently, an equilibrium crystallization would yield the same smooth zoning pattern for any *P–T* path involving continuous garnet growth, whatever the exact shape of the path. It is then necessary to call on kinetic factors to explain the observed type of garnet 2 zoning. These may be related, for instance, to an accelerated exhumation rate between M_{A1} and M_{A2} when garnet growth failed to keep pace with the evolution of *P–T* conditions.

The small garnet 2 crystals and overgrowths on garnet 1 therefore record a *P–T* evolution at decreasing pressure and slightly increasing temperature. This result is at variance with the *P–T* path proposed by Ballèvre (1988), who suggested a near-isothermal decompression, as well as Borghi *et al.* (1996), who argued that two generations of Alpine garnet were present, recording the pressure peak and a late temperature increase, respectively, after initial decompression and cooling. Two arguments against the latter hypothesis are as follows.

First, the evidence presented by Borghi *et al*. (1996) is open to question because the three garnet generations do not occur in the same rock. Specifically, the authors recognized pre-Alpine garnet with Alpine overgrowths in the Tsésère micaschists, an observation confirmed by our study. Nevertheless, the third garnet generation was found in another rock type, and its identification is mainly based on its difference in chemistry with respect to both garnet 1 and garnet 2. We consider that this difference is due to the bulk-rock chemistry, hence the different mol.% as well as chemical composition of garnet. Several garnet generations cannot be distinguished using observations from rocks with different bulk chemistries.

Second, on decompression, the mol.% of garnet in the calculated pseudosection increases with increasing temperature (Fig. 12). This means that: (i) any decrease in temperature during decompression would have been accompanied by garnet dissolution and (ii) any late increase in temperature, at pressures lower than 10 kbar, would have been recorded by garnet as well as biotite growth. However, biotite growth is accompanied by a moderate dissolution (rather than growth) of garnet in our samples.

The occurrence of two, rather than three, garnet generations is consistent with studies in other Penninic units, like the Dora-Maira (Matsumoto & Hirajima, 2000), where the samples studied are closely similar to those used in the present study.

CONCLUSIONS

1 The garnet–chloritoid micaschists from the Gran Paradiso Unit contain multi-stage garnet, with relics of an early, high-temperature event of pre-Alpine age present as cores of large garnet, later fractured and partly dissolved, and narrow overgrowths and newly grown garnet of small size, of Alpine age. This observation is consistent with previous reports in the Gran Paradiso Unit (Borghi & Sandrone, 1995) as well as many other pre-Alpine basements in the Western Alps (Fig. 1).

2 Growth zoning is preserved in both generations of garnet, suggesting that garnet 1 grew at increasing temperature and slightly increasing pressure, whereas garnet 2 grew at slightly increasing temperature and decreasing pressure. Estimated *P–T* conditions are of ~620 °C, 6 kbar for the peak of the pre-Alpine event, and 490 °C, 18–20 kbar for the pressure peak of the Alpine event.

3 No evidence for a third garnet generation has been found in these samples. Interpretation of the growth zoning of garnet 2 using calculated pseudosections does not record an isothermal decompression (Ballèvre, 1988) nor does it record decreasing temperature at decreasing pressure, followed by a late, nearly isobaric, increase in temperature suggested by Borghi *et al*. (1996) and Brouwer *et al*. (2002). Our interpretation, therefore, does not support the existence of a late thermal pulse due to mantle delamination proposed by Brouwer *et al*. (2004).

4 Preservation of growth zoning in both generations of garnet and the limited amount of diffusive re-equilibration at the boundary between the two garnets indicate that either temperature was too low during the Alpine history or that these rocks were subjected to a fast burial and exhumation rate (cf. Faryad & Chakraborty, 2005).

ACKNOWLEDGEMENTS

X. Le Coz is acknowledged for making the numerous thin sections required by our study in the Gran Paradiso, Those used in this paper representing only a small fraction of the material accumulated over the last 3 years. We are grateful to M. Racek for discussions concerning the modelling of some high-pressure phase relations. The paper benefited from detailed constructive reviews by A. Proyer and two anonymous reviewers. Editorial handling by M. Brown is greatly appreciated.

REFERENCES

Ballèvre, M., 1988. Collision continentale et chemins *P–T*: L'unité pennique du Grand Paradis (Alpes occidentales). *Mémoires et Documents du Centre Armoricain d'Etudes Structurales des Socles*, **19,** 352 p.

Battiston, P., Benciolini, L., Dal Piaz, G. V., *et al*., 1984. Geologia di una traversa dal Gran Paradiso alla zona Sesia-Lanzo in alta Val Soana, Piemonte. *Memorie della Società Geologica Italiana*, **29,** 209–232.

Bearth, P., 1952. Geologie und Petrographie des Monte Rosa. *Beiträge zur Geologische Karte der Schweiz (Neue Folge)*, **96,** 1–94.

Benciolini, L., Martin, S. & Tartarotti, P., 1984. Il metamorfismo eclogitico nel basamento del Gran Paradiso ed in unità piemontesi della valle di Campiglia. *Memorie della Società Geologica Italiana*, **29,** 127–151.

Bertrand, M., 1894. Etudes dans les Alpes françaises (structure en éventail, massifs amygdaloïdes et métamorphisme). *Bulletin de la Société Géologique de France*, **3**(XXII), 69–162.

Bertrand, J.-M., Pidgeon, R. T., Leterrier, J., Guillot, F., Gasquet, D. & Gattiglio, M., 2000. SHRIMP and IDTIMS U-Pb zircon ages of the pre-Alpine basement in the internal Western Alps (Savoy and Piemont). *Schweizerische Mineralogische und Petrographische Mitteilungen*, **80,** 225–248.

Biino, G. & Pognante, U., 1989. Paleozoic continental-type gabbros in the Gran Paradiso nappe (western Alps, Italy): early-Alpine eclogitization and geochemistry. *Lithos*, **24,** 3–19.

Bocquet, J., 1974. Le socle Briançonnais de Vanoise (Savoie): arguments en faveur de son âge anté-alpin et de son polymétamorphisme. *Comptes Rendus de l'Académie des Sciences de Paris*, **278**(D), 2601–2604.

Borghi, A. & Sandrone, R., 1995. Petrological constraints on the Alpine *P–T* history of the internal Pennine nappes of the Western Alps. *Bollettino del Museo Regionale di Scienze Naturali (Torino), Supplemento*, **13,** 241–272.

Borghi, A., Cadoppi, P., Porro, A. & Sacchi, R., 1985. Metamorphism in the north part of the Dora-Maira Massif (Cottian Alps). *Bollettino del Museo Regionale di Scienze Naturali, Torino*, **3,** 369–380.

Borghi, A., Compagnoni, R. & Sandrone, R., 1996. Composite *P–T* paths in the Internal Penninic Massifs of the Western

Alps: petrological constraints to their thermo-mechanical evolution. *Eclogae Geologicae Helvetiae*, **89,** 345–367.
Bouffette, J., Lardeaux, J.-M. & Caron, J.-M., 1993. Le passage des granulites aux éclogites dans les métapélites de l'unité de la Punta Muret (Massif Dora-Maira, Alpes occidentales). *Comptes Rendus de l'Académie des Sciences de Paris*, **II 317,** 1617–1624.
Brouwer, F. M., 2000. Thermal evolution of high-pressure metamorphic rocks in the Alps. *Geologica Ultraiectina*, **1999,** 221 p.
Brouwer, F. M., Vissers, R. L. M. & Lamb, W. M., 2002. Structure and metamorphism of the Gran Paradiso massif, western Alps, Italy. *Contributions to Mineralogy and Petrology*, **143,** 450–470.
Brouwer, F. M., Van de Zedde, M. J. R., Wortel, M. J. R. & Vissers, R. L. M., 2004. Late orogenic heating during exhumation: Alpine *P–T*-t trajectories and thermomechanical models. *Earth and Planetary Science Letters*, **220,** 185–199.
Burri, M., 1983. Description géologique du front du Saint-Bernard dans les vallées de Bagnes et d'Entremont (Valais). *Bulletin de Géologie de Lausanne*, **270,** 1–88.
Callegari, E., Compagnoni, R. & Dal Piaz, G. V., 1969. Relitti di strutture intrusive erciniche e scisti a sillimanite nel Massicio del Gran Paradiso. *Bollettino della Società Geologica Italiana*, **88,** 59–69.
Chopin, C., 1981. Mise en évidence d'une discontinuité du métamorphisme alpin entre le massif du Grand Paradis et sa couverture allochtone (Alpes occidentales française). *Bulletin de la Société Géologique de France*, **23,** 297–301.
Choukroune, P. & Gapais, D., 1983. Strain pattern in the Aar granites (Central Alps): orthogneiss developed by bulk inhomogeneous flattening. *Journal of Structural Geology*, **5,** 411–418.
Coggon, R. & Holland, T. J. B., 2002. Mixing properties of phengitic micas and revised garnet-phengite thermobarometers. *Journal of Metamorphic Geology*, **20,** 683–696.
Compagnoni, R., 1977. The Sesia-Lanzo zone: high pressure-low temperature metamorphism in the Austroalpine continental margin. *Rendiconti della Società Italiana di Mineralogia e Petrologia*, **33,** 335–374.
Compagnoni, R. & Lombardo, B., 1974. The Alpine age of the Gran Paradiso eclogites. *Rendiconti della Società Italiana di Mineralogia e Petrologia*, **30,** 223–237.
Compagnoni, R. & Prato, R., 1969. Paramorfosi di cianite su sillimanite in scisti pregranitici del massicio del Gran Paradiso. *Bollettino della Società Geologica Italiana*, **88,** 537–549.
Compagnoni, R., Elter, G. & Lombardo, B., 1974. Eterogeneita stratigrafica del complesso degli "gneiss minuti" nel massiccio cristallino del Gran Paradiso. *Memorie della Società Geologica Italiana*, **13** (Suppl.1)**,** 227–239.
Dachs, E. & Proyer, A., 2001. Relics of high-pressure metamorphism from the Grossglockner region, Hohe Tauern, Austria: paragenetic evolution and *P–T* paths of retrogressed eclogites. *European Journal of Mineralogy*, **13,** 67–86.
Dal Piaz, G. V., 1963. Il cristallino antico del versante meridionale del Monte Rosa: paraderivati a prevalente metamorfismo Alpino. *Rendiconti della Società Italiana di Mineralogia*, **20,** 102–135.
Dal Piaz, G. V., 1966. Gneiss ghiandoni, marmi ed anfiboliti antiche del ricoprimento Monte Rosa nell'alta Valle d'Ayas. *Bollettino della Società Geologica Italiana*, **85,** 103–132.
Dal Piaz, G. V., 1993. Evolution of Austro-Alpine and Upper Penninic basement in the northwestern Alps from Variscan convergence to post-Variscan extension. In: *Pre-Mesozoic Geology in the Alps* (eds von Raumer, J. F. & Neubauer, F.), pp. 249–265. Springer-Verlag, Berlin.
Dal Piaz, G. V. & Lombardo, B., 1986. Early Alpine eclogite metamorphism in the Penninic Monte Rosa–Gran Paradiso basement of the northwestern Alps. In: *Blueschists and Eclogites, Geological Society of America Memoir 164* (eds Evans, B. W. & Brown, E. H.), pp. 249–265. Geological Society of America, Boulder, CO.
Dal Piaz, G. V., Lombardo, B. & Gosso, G., 1983. Metamorphic evolution of the Mt. Emilius klippe, Dent Blanche nappe, Western Alps. *American Journal of Science*, **283-A,** 438–458.
Dale, J. & Holland, T. J. B., 2003. Geothermobarometry, *P–T* paths and metamorphic field gradients of high-pressure rocks from the Adula Nappe, Central Alps. *Journal of Metamorphic Geology*, **21,** 813–829.
Dale, J., Powell, R., White, R. W., Elmer, F. L. & Holland, T. J. B., 2005. A thermodynamic model for Ca-Na clinoamphiboles in Na_2O-CaO-FeO-MgO-Al_2O_3-SiO_2-H_2O-O for petrological calculations. *Journal of Metamorphic Geology*, **23,** 771–791.
Desmons, J., 1992. The Briançon basement (Pennine Western Alps): mineral composition and polymetamorphic evolution. *Schweizerische Mineralogische und Petrographische Mitteilungen*, **72,** 37–55.
Desmons, J. & Ghent, E. D., 1977. Chemistry, zonation and distribution coefficients of elements in eclogitic minerals from the Eastern Sesia Unit, Italian Western Alps. *Schweizerische Mineralogische und Petrographische Mitteilungen*, **57,** 397–411.
Desmons, J., Laduron, D. & De Béthune, P., 1977. Grenats zonés de la nappe du Grand-saint-Bernard et de la zone piémontaise (Alpes Occidentales). *Mémoires de l'Institut géologique de l'Université de Louvain*, **29,** 327–347.
Desmons, J., Compagnoni, R. & Cortesogno, L., 1999a. Alpine metamorphism of the western Alps : II. High-P/T and related pre-greenschist metamorphism. *Schweizerische Mineralogische und Petrographische Mitteilungen*, **79,** 111–134.
Desmons, J., Compagnoni, R., Cortesogno, L., Frey, M. & Gaggero, L., 1999b. Pre-alpine metamorphism of the internal zones of the Western Alps. *Schweizerische Mineralogische und Petrographische Mitteilungen*, **79,** 23–39.
Detraz, G. & Loubat, H., 1984. Faciès à disthène, staurotide et grenat dans un micaschiste appartenant à l'unité des "gneiss du Sapey" (Vanoise, Alpes françaises). *Géologie alpine*, **60,** 5–12.
Engvik, A. K., Austrheim, H. & Andersen, T. B., 2000. Structural, mineralogical and petrophysical effects on deep crustal rocks of fluid-limited polymetamorphism, Western Gneiss Region, Norway. *Journal of the Geological Society of London*, **157,** 121–134.
Erambert, M. & Austrheim, H., 1993. The effect of fluid and deformation on zoning and inclusion patterns in poly-metamorphic garnets. *Contributions to Mineralogy and Petrology*, **115,** 204–214.
Ernst, W. G., 1973. Interpretative synthesis of metamorphism in the Alps. *Geological Society of America Bulletin*, **84,** 2053–2078.
Faryad, S. W. & Chakraborty, S., 2005. Duration of Eo-Alpine metamorphic events obtained from multicomponent diffusion modelling of garnet: a case study from the Eastern Alps. *Contributions to Mineralogy and Petrology*, **150,** 306–318.
Faryad, S. W. & Hoinkes, G., 2003. P-T gradient of Eo-Alpine metamorphism within the Austroalpine basement units east of the Tauern Window (Austria). *Mineralogy and Petrology*, **77,** 129–159.
Frey, M., Hunziker, J. C., Frank, W. *et al.*, 1974. Alpine metamorphism of the Alps: a review. *Schweizerische Mineralogische und Petrographische Mitteilungen*, **54,** 247–290.
Ganne, J., Bussy, F. & Vidal, O., 2003. Multi-stage garnet in the internal Briançonnais basement (Ambin Massif, Savoy): New petrological constraints on the blueschist-facies metamorphism in the Western Alps and tectonic implications. *Journal of Petrology*, **44,** 1281–1308.
Giorgis, D., Thélin, P., Stampfli, G. & Bussy, F., 1999. The Mont-Mort metapelites: Variscan metamorphism and geodynamic context (Briançonnais basement, Western Alps, Switzerland). *Schweizerische Mineralogische und Petrographische Mitteilungen*, **79,** 381–398.
Guiraud, M., Powell, R. & Rebay, G., 2001. H_2O in metamorphism and unexpected behaviour in the preservation of metamorphic mineral assemblages. *Journal of Metamorphic Geology*, **19,** 445–454.

Heinrich, C. A., 1986. Eclogite facies regional metamorphism of hydrous mafic rocks in the Central Alpine Adula Nappe. *Journal of Petrology*, **27,** 123–154.

Hiroi, Y. & Ellis, D., 1994. Preservation of Ca, P, REE growth zonation patterns in garnet which have undergone partial Fe, Mg and Mn volume diffusion re-equilibration: examples from Japan and Sri Lanka. *EOS, Transactions of the American Geophysical Union*, **75,** 185–186.

Holland, T. J. B. & Powell, R., 1996. Thermodynamics of order-disorder in minerals: II. Symmetric formalism applied to solid solutions. *American Mineralogist*, **81,** 1425–1437.

Holland, T. J. B. & Powell, R., 1998. An internally consistent thermodynamic data set for phases of petrological interest. *Journal of Metamorphic Geology*, **16,** 309–343.

Holland, T. & Powell, R., 2003. Activity–composition relations for phases in petrological calculations: an asymmetric multicomponent formulation. *Contributions to Mineralogy and Petrology*, **145,** 492–501.

Hy, C., 1984. Métamorphisme polyphasé et évolution tectonique dans la croûte continentale éclogitisée: les séries granitiques et pélitiques du Monte Mucrone. (zone Sesia-Lanzo, Alpes Italiennes). PhD Thesis, Université Pierre et Marie Curie, Paris, 199 p.

Karabinos, P., 1984. Polymetamorphic garnet zoning from Southeastern Vermont. *American Journal of Science*, **284,** 1008–1025.

Laduron, D. & Desmons, J., 1981. Résorption et néocroissances dans les grenats d'un micaschiste du Ruitor (Alpes penniques franco-Italiennes). *Mémoires de l'Institut géologique de l'Université de Louvain*, **31,** 335–347.

Lanzirotti, A., 1995. Yttrium zoning in metamorphic garnets. *Geochimica et Cosmochimica Acta*, **59,** 4105–4110.

Lardeaux, J.-M. & Spalla, M. I., 1991. From granulites to eclogites in the Sesia zone (Italian Western Alps): a record of the opening and closure of the Piedmont ocean. *Journal of Metamorphic Geology*, **9,** 35–59.

Lardeaux, J.-M., Gosso, G., Kienast, J.-R. & Lombardo, B., 1982. Relations entre le métamorphisme et la déformation dans la zone de Sesia-Lanzo (Alpes occidentales) et le problème de l'éclogitisation de la croûte continentale. *Bulletin de la Société géologique de France*, **24,** 793–800.

Le Bayon, R., 2003. Tectono-Metamorphic Evolution of the Monte Rosa Nappe and Surrounding Units (Western Alps): Implications for Alpine Geodynamics and Exhumation of Metamorphic Terranes. PhD Thesis, Universität Basel, Basel.

Le Bayon, B. & Ballèvre, M., 2004. Field and petrological evidence for a Late Palaeozoic (Upper Carboniferous–Permian) age of the Erfaulet orthogneiss (Gran Paradiso, Western Alps). *Comptes Rendus Geoscience*, **336,** 1079–1089.

Le Bayon, B. & Ballèvre, M., 2006. Deformation history of a subducted continental crust (Gran Paradiso, Western Alps): continuing crustal shortening during exhumation. *Journal of Structural Geology*, **28,** 793–815.

Leloup, P. H., Arnaud, N., Sobel, E. R. & Lacassin, R., 2005. Alpine thermal and structural evolution of the highest external crystalline massif: The Mont Blanc. *Tectonics*, **24,** TC4002.

Loomis, T. P., 1983. Compositional zoning of crystals: a record of growth and reaction history. In: *Kinetics and Equilibrium in Minerals Reaction, Advances in Physical Geochemistry 3* (ed. Saxena, S. K.), pp. 1–60. Springer-Verlag, New York.

Madhjoub, Y., Choukroune, P. & Kiénast, J.-R., 1997. Kinematics of a complex Alpine segment: superimposed tectonic and metamorphic events in the Petite Kabylie Massif (northern Algeria). *Bulletin de la Société Géologique de France*, **168,** 649–661.

Malusà, M. G., 2005. The Gran San Bernardo nappe in the Aosta valley (western Alps): a composite stack of distinct continental crust units. *Bulletin de la Société Géologique de France*, **176,** 417–431.

Matsumoto, N. & Hirajima, T., 2000. Garnet in pelitic schists from a quartz-eclogite unit of the southern Dora-Maira massif, Western Alps. *Schweizerische Mineralogische und Petrographische Mitteilungen*, **80,** 53–62.

Meffan-Main, S., Cliff, R. A., Barnicoat, A. C., Lombardo, B. & Compagnoni, R., 2004. A Tertiary age for Alpine high-pressure metamorphism in the Gran Paradiso, western Alps: a Rb-Sr microsampling study. *Journal of Metamorphic Geology*, **22,** 267–281.

Perchuk, A. L., Burchard, M., Maresch, W. V. & Schertl, H.-P., 2005. Fluid-mediated modification of garnet interiors under ultrahigh-pressure conditions. *Terra Nova*, **17,** 545–553.

Pognante, U., Talarico, U., Rastelli, N. & Ferrati, N., 1987. High pressure metamorphism in the nappes of the valle dell'Orco traverse (Western Alps collisional belt). *Journal of Metamorphic Geology*, **5,** 397–414.

Powell, R. & Holland, T. J. B., 1988. An internally consistent dataset with uncertainties and correlations: 3. Applications to geobarometry, worked examples and a computer program. *Journal of Metamorphic Geology*, **6,** 173–204.

Powell, R. & Holland, T., 1999. Relating formulations of the thermodynamics of mineral solid solutions: activity modeling of pyroxenes, amphiboles, and micas. *American Mineralogist*, **84,** 1–14.

Proyer, A., 2003. The preservation of high-pressure rocks during exhumation: metagranites and metapelites. *Lithos*, **70,** 183–194.

von Raumer, J. F. & Bussy, F., 2004. Mont Blanc and Aiguilles Rouges; Geology of their polymetamorphic basement (External Massifs, Western Alps, France–Switzerland). *Mémoires de Géologie (Lausanne)*, **42,** 203 p.

von Raumer, J. F. & Schwander, H. W., 1985. Garnet evolution in pre-Variscan pelitic rocks from the Lake Emosson area, Aiguilles Rouges Massif, Western Alps. *Journal of Metamorphic Geology*, **3,** 467–479.

Rebay, G. & Spalla, M. I., 2001. Emplacement at granulite facies conditions of the Sesia-Lanzo metagabbros: an early record of Permian rifting? *Lithos*, **58,** 85–104.

Robinson, P., 1991. The eye of the petrographer, the mind of the petrologist. *American Mineralogist*, **76,** 1781–1810.

Rubatto, D. & Hermann, J., 2001. Exhumation as fast as subduction? *Geology*, **29,** 3–6.

Rubatto, D., Schaltegger, U., Lombardo, B., Colombo, F. & Compagnoni, R., 2001. Complex paleozoic magmatic and metamorphic evolution in the Argentera Massif (Western Alps) resolved with U-Pb dating. *Schweizerische Mineralogische und Petrographische Mitteilungen*, **81,** 213–228.

Rumble, D. III & Finnerty, T. A., 1974. Devonian grossular-spessartine overgrowths on Ordovician Almandine from Eastern Vermont. *American Mineralogist*, **59,** 558–562.

Sandrone, R. & Borghi, A., 1992. Zoned garnets in the northern Dora-Maira Massif and their contribution to a reconstruction of the regional metamorphic evolution. *European Journal of Mineralogy*, **4,** 465–474.

Spear, F. & Kohn, M., 1996. Trace element zoning in garnet as monitor of crustal melting. *Geology*, **24,** 1099–1102.

Thélin, P., 1992. Les métapélites du Mont-Mort: une fenêtre métamorphique (Nappe des Pontis, Zone du Ruitor, Valais). *Bulletin de Géologie de Lausanne*, **315,** 99–116.

Tracy, R. J., 1982. Compositional zoning and inclusions in metamorphic minerals. In: *Characterization of Metamorphism through Mineral Equilibria, Reviews in Mineralogy 10* (ed. Ferry, J. M.), pp. 355–397. Mineralogical Society of America, Washington, DC.

Vidal, O., Parra, T. & Trotet, F., 2001. A thermodynamic model for Fe-Mg aluminous chlorite using data from the equilibrium experiments and natural pelitic assemblages in the 100° to 600°C, 1 to 25 kb range. *American Journal of Science*, **301,** 557–592.

Vry, J. K., Baker, J., Maas, R., Little, T. A., Grapes, R. & Dixon, M., 2004. Zoned (Cretaceous and Cenozoic) garnet and the timing of high grade metamorphism, Southern Alps, New Zealand. *Journal of Metamorphic Geology*, **22,** 137–157.

Vuichard, J. P. & Ballèvre, M., 1988. Garnet-chloritoid equilibria in eclogitic-pelitic rocks from the Sesia zone (Western

Alps): their bearing on phase relations in high-pressure metapelites. *Journal of Metamorphic Geology*, **6,** 135–157.
Wei, C. & Powell, R., 2003. Phase relations in high-pressure metapelites in the system KFMASH (K_2O-FeO-MgO-Al_2O_3-SiO_2-H2O) with application to natural rocks. *Contribution to Mineralogy and Petrology*, **145,** 301–315.
Wei, C. & Powell, R., 2004. Calculated Phase Relations in High-Pressure Metapelites in the System NKFMASH (Na_2O-K_2O-FeO-MgO-Al_2O_3-SiO_2-H2O). *Journal of Petrology*, **45,** 183–202.
Wei, C. J. & Powell, R., 2006. Calculated phase relations in the system NCKFMASH (Na_2O-CaO-K_2O-FeO-MgO-Al_2O_3-SiO_2-H_2O) for high-pressure metapelites. *Journal of Petrology*, **47,** 385–408.
Wei, C. J., Powell, R. & Zhang, L. F., 2003. Eclogites from the south Tianshan, NW China: petrological characteristic and calculated mineral equilibria in the Na_2O-CaO-FeO-MgO-Al_2O_3-SiO_2-H_2O system. *Journal of Metamorphic Geology*, **21,** 163–179.
Whitney, D. L., 1991. Calcium depletion halos and Fe-Mn-Mg zoning around faceted plagioclase inclusions in garnet from high-grade pelitic gneiss. *American Mineralogist*, **76,** 493–500.
Wood, B. J., Hackler, R. T. & Dobson, D. P., 1994. Experimental determination of Mn-Mg mixing properties in garnet, olivine and oxide. *Contributions to Mineralogy and Petrology*, **115,** 438–448.

Received 23 November 2005; revision accepted 8 May 2006.

APPENDIX

Mixing models for solid–solution phases

Mineral mixing models and nonideality parameters are based on Holland & Powell (1998) and Powell & Holland (1999) and extended to the Mn-bearing system as described below. White mica are modelled after Coggon & Holland (2002), plagioclase after Holland & Powell (2003). The clinopyroxene (omphacite–jadeite) model, based on the study of Holland & Powell (1996), is that used in Wei *et al.* (2003).

Garnet

Variables: $x(g) = Fe/(Fe + Mg)$; $ca(g) = Ca/(Fe + Mg + Ca + Mn)$; $mn(g) = Mn/(Fe + Mg + Ca + Mn)$
Structural formulae of end-members:
Almandine (alm): $Fe_3Al_2Si_3O_8$
Pyrope (py): $Mg_3Al_2Si_3O_8$
Grossular (gr): $Ca_3Al_2Si_3O_8$
Spessartine (spss): $Mn_3Al_2Si_3O_8$
Site fractions: $X^M_{Fe} = x(1 - ca - mn)$; $X^M_{Mg} = (1 - x)(1 - ca - mn)$; $X^M_{Ca} = ca$; $X^M_{Mn} = mn$
Proportions: $p(alm) = x(1 - ca - mn)$; $p(py) = (1 - x)\ (1 - ca - mn)$; $p(gr) = ca$; $p(spss) = mn$
Nonideality: symmetric formalism; $w(alm,py) = 2.5$ kJ, $w(alm,gr) = 0$ kJ, $w(alm,spss) = 0$ kJ, $w(py,gr) = 33$ kJ, $w(py,spss) = 4.5$ kJ (Wood *et al.*, 1994), $w(gr,spss) = 0$ kJ

Staurolite

Variables: $x(st) = Fe/(Fe + Mg)$; $mn(st) = Mn/(Fe + Mg + Mn)$
Structural formulae of end-members:
Fe-staurolite (fst): $Fe_4Al_{18}Si_{7.5}O_{48}H_4$
Mg-staurolite (mst): $Mg_4Al_{18}Si_{7.5}O_{48}H_4$
Mn-staurolite (mnst): $Mn_4Al_{18}Si_{7.5}O_{48}H_4$
Site fractions: $X^M_{Fe} = x(1 - mn)$; $X^M_{Mg} = (1 - x)(1 - mn)$; $X^M_{Mn} = mn$
Proportions: $p(fst) = x(1 - mn)$; $p(mst) = (1 - x)(1 - mn)$; $p(mnst) = mn$
Nonideality: symmetric formalism; $w(fst,mst) = -8$ kJ, $w(fst,mnst) = 0$ kJ, $w(mst,mnst) = 0$ kJ

Chloritoid

Variables: $x(ctd) = Fe/(Fe + Mg)$; $mn(ctd) = Mn/(Fe + Mg + Mn)$
Structural formulae of end-members:
Fe-chloritoid (fctd): $FeAl_2SiO_5(OH)_2$
Mg-chloritoid (mctd): $MgAl_2SiO_5(OH)_2$
Mn-chloritoid (mnctd): $MnAl_2SiO_5(OH)_2$
Site fractions: $X^M_{Fe} = x(1 - mn)$; $X^M_{Mg} = (1 - x)(1 - mn)$; $X^M_{Mn} = mn$
Proportions: $p(fctd) = x(1 - mn)$; $p(mctd) = (1 - x)(1 - mn)$; $p(mnctd) = mn$
Nonideality: symmetric formalism; $w(fctd,mctd) = 1$ kJ, $w(fctd,mnctd) = 0$ kJ, $w(mctd,mnctd) = 0$ kJ

Chlorite

Variables: $x(chl) = $ bulk $Fe/(Fe + Mg)$; $mn(chl) = $ bulk $Mn/(Fe + Mg + Mn)$; $y(chl) = X^{T2}_{Al}$; $N(chl) = (X^{M4}_{Al} - X^{M1}_{Al})/2$
Structural formulae of end-members:
Al-free chlorite (afchl): $Mg_4MgMg[Si_2]Si_2O_{10}(OH)_4$
Clinochlore (clin): $Mg_4MgAl[SiAl]Si_2O_{10}(OH)_4$
Daphnite (daph): $Fe_4FeAl[SiAl]Si_2O_{10}(OH)_4$
Mn-chlorite (mnchl): $Mn_4MnAl[SiAl]Si_2O_{10}(OH)_4$
Amesite (ames): $Mg_4AlAl[Al_2]Si_2O_{10}(OH)_4$
Site fractions: $X^{M23}_{Fe} = x(1 - mn)$; $X^{M23}_{Mg} = (1 - x)(1 - mn)$; $X^{M23}_{Mn} = mn$; $X^{M1}_{Al} = y - N$; $X^{M1}_{Fe} = x(1 - mn)(1 - y + N)$; $X^{M1}_{Mg} = (1 - x)(1 - mn)(1 - y + N)$; $X^{M1}_{Mn} = mn(1 - y + N)$; $X^{M4}_{Al} = y + N$; $X^{M4}_{Mg} = (1 - x)(1 - mn)(1 - y - N)$; $X^{T2}_{Al} = y$; $X^{T2}_{Si} = 1 - y$
Proportions: $p(afchl) = 1 - y - N$; $p(clin) = 2N - 2x(1 - mn)(3 - y)/5 - 2\,mn(3 - y)/5$; $p(daph) = 2x(1 - mn)(3 - y)/5$; $p(mnchl) = 2\,mn(3 - y)/5$; $p(ames) = y - N$;
Nonideality: symmetric formalism; $w(afchl,clin) = 18$ kJ; $w(afchl,daph) = 14.5$ kJ; $w(afchl,mnchl) = 0$ kJ; $w(afchl,ames) = 20$ kJ; $w(clin,daph) = 2.5$ kJ; $w(clin,mnchl) = 0$ kJ; $w(clin,ames) = 18$ kJ; $w(daph,mnchl) = 0$ kJ; $w(daph,ames) = 13.5$ kJ; $w(mnchl,ames) = 0$ kJ

Biotite

Variables: $x(bi) = $ bulk $Fe/(Fe + Mg)$; $mn(bi) = $ bulk $Mn/(Fe + Mg + Mn)$; $y(bi) = X^{M1}_{Al}$; $Q(bi) = 3[x - (Fe/[Fe + Mg])^{M2}]$
Structural formulae of end-members:
Phlogopite (phl): $KMgMg_2[SiAl]Si_2O_{10}(OH)_2$
Annite (ann): $KFeFe_2[SiAl]Si_2O_{10}(OH)_2$
Mn-biotite (mnbi): $KMnMn_2[SiAl]Si_2O_{10}(OH)_2$
Eastonite (east): $KAlMg_2[Al_2]Si_2O_{10}(OH)_2$
"Ordered biotite" (obi): $KFeMg_2[SiAl]Si_2O_{10}(OH)_2$
Site fractions: $X^{M1}_{Al} = y$; $X^{M1}_{Fe} = x(1 - mn)(1 - y) + 2Q(1 - mn)/3)$; $X^{M1}_{Mg} = (1 - x)(1 - mn)(1 - y) - 2Q(1 - mn)/3)$; $X^{M1}_{Mn} = mn(1 - y)$; $X^{M2}_{Fe} = (x - Q/3)(1 - mn)$; $X^{M2}_{Mg} = (1 - x + Q/3)(1 - mn)$; $X^{M2}_{Mn} = mn$; $X^{T1}_{Al} = (1 + y)/2$; $X^{T1}_{Si} = (1 - y)/2$
Proportions: $p(phl) = (1 - x)(1 - mn)(1 - y) - 2\,mny/3 - 2Q(1 - mn)/3)$; $p(ann) = (1 - mn)(x - Q/3)$; $p(mnbi) = mn(3 - y)/3$; $p(east) = y$; $p(obi) = Q(1 - mn) - xy(1 - mn)$
Nonideality: symmetric formalism: $w(phl,ann) = 9$ kJ; $w(phl,mnbi) = 0$ kJ; $w(phl,east) = 10$ kJ; $w(phl,obi) = 3$ kJ; $w(ann, mnbi) = 0$ kJ; $w(ann,east) = -1$ kJ; $w(ann,obi) = 6$ kJ; $w(mnbi,east) = 0$ kJ; $w(mnbi,obi) = 0$ kJ; $w(east,obi) = 10$ kJ; DQF: $I^{bi}_{obi} = -10.73$ kJ